







Dynamics of edge modes in monitored Su-Schrieffer-Heeger Models

Giulia Salatino ¹, Gianluca Passarelli ², Angelo Russomanno ²,
Giuseppe E. Santoro ^{3,4}, Procolo Lucignano ² and Rosario Fazio ^{4,2}

¹*Scuola Superiore Meridionale, Via Mezzocannone, 4 80138, Napoli, Italy.*^a

²*Dipartimento di Fisica E. Pancini, Università di Napoli "Federico II",*

Complesso di Monte S. Angelo, via Cinthia, I-80126 Napoli, Italy

³*SISSA, Via Bonomea 265, I-34136 Trieste, Italy.*

⁴*The Abdus Salam International Centre for Theoretical Physics, I-34014 Trieste, Italy*

(Dated: March 14, 2025)

We investigate the effect of dissipation on the dynamics of edge modes in the monitored Su-Schrieffer-Heeger (SSH) model. Our study considers both a linear observable and a nonlinear entanglement measure, namely the two-point correlation function and the Disconnected Entanglement Entropy (DEE), as diagnostic tools. While dissipation inevitably alters the entanglement properties observed in the closed system, statistical analysis of quantum trajectories reveals that by protecting the chain's edges from dissipation, it is possible to recover characteristic features analogous to those found in the unitary limit. This highlights the fundamental role of spatial dissipation patterns in shaping the dynamics of edge modes in monitored systems.

I. INTRODUCTION

Condensed matter physics has seen significant advancements from the discovery and investigation of systems characterized by non-trivial topological phases [1]. While the main focus has been centered in the study to the ground state of both free and interacting many-body systems, recent attention has been devoted to understand topological properties of non-Hermitian [2, 3] and open quantum systems governed by Lindblad dynamics [4–7], where the interplay between topology and non-unitary dynamics gives rise to novel phases and dynamics not observed in closed systems. Examples are the breakdown of bulk-boundary correspondence and the emergence of the non-Hermitian skin effect [2]. Symmetries play a crucial role in determining the topological properties of these systems and the tenfold way classification, based on Altland-Zirnbauer classes [8] has been extended to the steady-state of systems governed by non-Hermitian [9, 10] and Lindblad [6, 7, 11–16] dynamics. Still, defining a suitable topological marker for open topological insulators remains an open challenge. Several quantities have been proposed, including non-Hermitian topological invariants [17–19], the Uhlmann phase [20–22], the ensemble geometric phase [23, 24], the mixed-state topological order parameter of [25], the long-time entanglement negativity [26], as well as the imbalance and current properties [27, 28].

Inspired by these studies on the interplay of decoherence/dissipation and topology, aim of the present work is to investigate the topological properties of monitored quantum systems, i.e. a stochastic dynamics given by a smooth evolution interrupted by quantum jumps [29–33], and whose average quantum state (the density matrix) is governed by the Lindblad equation. More specifically,

we will analyze the dynamics of topological edge states under the combined effect of a quantum quench *and* the random fluctuations induced by quantum jumps.

Very recently, monitored dynamics of many-body systems has been actively started to be investigated in quantum circuits and open systems. Two independent works [34, 35] showing the existence of a measurement-induced phase transition visible only at the level of single trajectories triggered an intense activity scrutinizing many different facets of this phenomenology (the interested reader can find additional references on this activities in the review articles [36] and [37]). In essence, by observing the system at the level of single trajectories (i.e. monitoring the systems) it is possible to have access to nonlinear functions of the quantum states, showing a plethora of new phenomena, that cannot be extracted by looking at the density matrix. This is the case of topological markers.

Indeed, averaging over trajectories is *not* equivalent to the study of the topology embedded in the density matrix because the topological markers are usually nonlinear functions of the quantum states. This means that looking at monitored systems we are able to probe the interplay of topology and dissipation from a new angle. The protocol we follow, on the other hand, is rather standard, that of a quantum quench. After having prepared the system in a given quantum states (topological or trivial) we will follow the evolution of the signatures of topology along a given trajectory, where the smooth (non-Hermitian) evolution is interrupted at random times by quantum jumps. We do not confine ourselves to the steady-state, on the contrary we are interested in understanding how these properties evolve in time, along a given quantum trajectory, and subject both to Hamiltonian evolution and dissipation/decoherence.

A key aspect to bear in mind is the fact that along a single trajectory the state is always pure and therefore we can use topological markers that have been devised for the unitary case. For this reason, after a prelim-

^a giulia.salatino@unina.it

inary analysis of the two-point correlator between the edge sites of the chain, we move on and study a quantity that is nonlinear in the density matrix of the system, namely the Disconnected Entanglement Entropy (DEE), first introduced in Ref. [38]. DEE is a robust measure of symmetry-protected topological phases, while traditional entanglement measures, such as the von Neumann entropy, fall short [39–43]. Unlike the winding number, the DEE is not a bulk topological invariant. Instead, it quantifies the entanglement between topological edge states by partitioning the system into disjoint regions and measuring the entropy of the reduced density matrix for these regions. DEE has been shown to detect long-range entanglement in certain phases that are not symmetry-protected topological phases [44], as well as Majorana zero modes in semiconductor-superconductor heterostructures [45]. This order parameter, closely related to entanglement entropy, is also experimentally accessible, as discussed in Refs. [46–48]. Of particular relevance for the present work, are Refs. 49–51 where the dynamics of the DEE is considered, here extended to the stochastic dynamics of quantum jumps.

We investigate a paradigmatic case, the Su-Schrieffer-Heeger (SSH) model, well-known for its simplicity and the rich variety of phenomena it presents. Initially proposed to describe electron behavior in polyacetylene [52, 53], it serves as a one-dimensional example of a system with topological edge states protected by chiral symmetry [54, 55]. Specifically, we examine the DEE of an SSH chain under different types of dissipation, classified according to Ref. [6].

We first examine the time evolution of the average value of the DEE over multiple trajectories. Then, we perform a statistical analysis of individual trajectories, focusing on the variation of the DEE caused by each quantum jump in the initial phase of the dynamics. We consider both uniform and non-uniform types of dissipation, acting differently on different segments of the chain.

Our results show that while bulk dissipation has a limited impact on the system, quantum jumps at the boundaries, as expected, have a disruptive effect on the edge modes. These results emerge both in the average properties and in the fluctuations of the DEE.

On one hand, through the study of the average value of the DEE, we extend the results of [50], where it was shown that an initial doublet of entangled topological modes persists for a time linear in the system size when evolving under a local Hamiltonian. Indeed, here we extend this result to quadratic dissipators, demonstrating that the entanglement of the topological modes remains for a time linear in system size as long as the dissipator does not affect the boundary. Notably, in the transient regime of the dynamics, the spatial localization of the dissipation plays a more crucial role than its symmetry class in determining the stability of the edge modes. Furthermore, when dissipation affects the boundary of the chain, the dynamics induced by the coherent part of the Lindbladian also appears to be crucial.

On the other hand, the statistical analysis reveals that, when the quantum jumps are localized, there is a peak in the probability distribution of the DEE variation that signals the destruction of the topological entanglement. This peak is primarily attributable to the effect of the first local jump occurring on one of the two edge sites.

The paper is organized as follows: In Section II, we review the SSH model and its topological properties, introduce the types of dissipative dynamics we will examine, describe the quantum jump unraveling of the Lindblad equation, and outline our methodology for calculating the DEE. In Section III, we present the DEE and the method to calculate its time evolution. In Section IV, we discuss our main results, including the effects of different dissipative dynamics on the edge modes characterizing the system’s initial topological phase. We also explore the time evolution of the DEE and the scaling behavior of a DEE-related quantity: the time at which the DEE deviates from its quantized initial value due to dissipation. Lastly, we conduct a statistical analysis of the DEE’s variation after a quantum jump, considering both the timing and location of the jump for a comprehensive time- and index-resolved analysis. In Section V, we discuss the implications of our findings for the understanding of dissipation in topological phases and propose potential directions for future research.

II. THE MODEL AND ITS MONITORED DYNAMICS

As mentioned in the Introduction, we will focus our attention on a one-dimensional free-fermion model governed by the SSH Hamiltonian. The Hamiltonian of the SSH model \hat{H}_{SSH} describes a 1D atomic chain with two atoms per unit cell, on which electrons hop with staggered hopping amplitude [56]. The sites of the lattice $i \equiv (j, A/B)$ are identified by their coordinates j in one of the two sub-lattices A/B . In the following, we will study the dynamics of the monitored system along a quantum trajectory [29–33]. In this case, the dynamics, under the action of the environment, is given by a smooth evolution, governed by non-Hermitian Hamiltonian, interrupted by quantum jumps described by the corresponding Lindblad operators \hat{L}_i .

II.1. Stochastic dynamics and Quantum jumps

The stochastic Schrödinger equation, governing the wavefunction $|\psi(t)\rangle$, has the form ($\hbar = 1$)

$$d|\psi(t)\rangle = \left\{ dt \left(-i\hat{H}_{\text{eff}} + \frac{1}{2} \sum_i \langle \hat{L}_i^\dagger \hat{L}_i \rangle \right) + \sum_i dN_i(t) \left(\frac{\hat{L}_i}{\sqrt{\langle \hat{L}_i^\dagger \hat{L}_i \rangle_t}} - \hat{\mathbb{1}} \right) \right\} |\psi(t)\rangle, \quad (1)$$

where we define $\langle \hat{L}_i^\dagger \hat{L}_i \rangle_t = \langle \psi(t) | \hat{L}_i^\dagger \hat{L}_i | \psi(t) \rangle$. In Eq. (1), the term $-i\hat{H}_{\text{eff}} |\psi(t)\rangle dt$ gives a deterministic contribution to the evolution of the state with a non-Hermitian Hamiltonian of the form

$$\hat{H}_{\text{eff}} = \hat{H}_{\text{SSH}} - \frac{i}{2} \sum_i \hat{L}_i^\dagger \hat{L}_i, \quad (2)$$

the c-number term in the first bracket is needed in order to keep the state normalized. The second term on the r.h.s. — the fluctuation term — is the one that makes the differential equation stochastic. Indeed, $dN_i(t) = N_i(t + dt) - N_i(t)$ represents the number of *jumps* of type i the state goes across as a result of a *measurement* made by the environment in the time interval dt . This is a stochastic variable with expectation value

$$\text{E}[dN_i(t)] = \langle \hat{L}_i^\dagger \hat{L}_i \rangle_t dt. \quad (3)$$

Since we consider $dt \rightarrow 0$, we can assume $dN_i(t)$ will follow a Poissonian distribution [57], so that

$$dN_i(t) = \begin{cases} 1 & \text{with probability } \langle \hat{L}_i^\dagger \hat{L}_i \rangle_t dt \\ 0 & \text{with probability } 1 - \langle \hat{L}_i^\dagger \hat{L}_i \rangle_t dt \end{cases}. \quad (4)$$

The stochastic noise acting on each trajectory can be seen as a result of action (generalized measurement) of the environment on the systems.

Each realization of this stochastic process is a quantum trajectory, the ensemble (average state) evolution being provided by the Lindblad equation [33, 58]

$$\frac{d}{dt} \hat{\rho}(t) = -i[\hat{H}_{\text{SSH}}, \hat{\rho}(t)] + \sum_i \left(\hat{L}_i \hat{\rho}(t) \hat{L}_i^\dagger - \frac{1}{2} \{ \hat{L}_i^\dagger \hat{L}_i, \hat{\rho}(t) \} \right). \quad (5)$$

As long as one is interested in the evolution of physical observables, the averaging over the trajectories or the study of the Lindblad dynamics is equivalent (the advantage of the unraveling method is that it requires evolving a pure state instead of a density matrix, resulting in a substantial reduction in computational complexity). The situation changes drastically when one is interested in signatures that are embodied in quantities that are nonlinear function of the quantum states. Topological markers are an example of this sort. In this case following the dynamics of topological properties of a monitored quantum system may differ considerably from the topological properties of its average dynamics. This is what we are going to study in the next Sections.

II.2. The model

The Hamiltonian of the systems, defined on a one-dimensional lattice with open boundary conditions

(OBC), is

$$\hat{H}_{\text{SSH}} = -J_o \sum_{j=1}^N \hat{c}_{j,A}^\dagger \hat{c}_{j,B} - J_e \sum_{j=1}^{N-1} \hat{c}_{j+1,A}^\dagger \hat{c}_{j,B} + \text{h.c.}, \quad (6)$$

where $J_o, J_e > 0$, A and B indicate the type of atom within the unit cell (the sublattice index), N is the number of unit cells and $L = 2N$ is the number of sites in the chain. At half filling, the ground state of \hat{H}_{SSH} displays two distinct topological phases. When $J_o/J_e > 1$ the phase is topologically trivial, while it is topological for $J_o/J_e < 1$. In the topological phase, the density profile of each edge shows one localized fermion on the left end and one on the right end of the chain – see sketch in Fig. 1(a), and Appendix A and Refs. [56, 59] for further details. This is related to the fact that, in this topological, fully-dimerized limit, one fermion is localized at each inter-cell link, and two unpaired fermions are left on the extreme sites.

In the thermodynamic limit these topological boundary excitations are degenerate and are at zero energy. For any finite size they hybridize, and an exponentially small gap open between the even and the odd superposition of them. Therefore at finite size, half filling and zero temperature – when all the lower band is occupied – only the even superposition $\frac{1}{\sqrt{2}} (\hat{c}_{N,B}^\dagger + \hat{c}_{1,A}^\dagger)$ of the topological boundary modes is occupied, while the odd is empty. This even superposition of edge modes can be written as a Bell state, as it is explained in detail in Appendix A and is such that the two distant edges are entangled. This is the only long-range entanglement of the whole chain that can be detected when the system is in a topological phase [50].

Beyond it, there is only short-range entanglement across each intercell link. The Hamiltonian of the SSH model (6) falls in the BDI symmetry class of the AZ tenfold way [8], which leads to a \mathbb{Z} type of topological invariant in 1D. This means that the edge states are protected by time-reversal, chiral and particle-hole symmetries and that there is an infinite countable number of distinct topological phases with the symmetries preserved (see also Appendix B). In the presence of periodic boundary conditions (PBC) translation symmetry allows to detect the topological phase using non-local topological invariants like the winding number or Zak phase in k space [60, 61].

The dynamics introduced in Eq. (1) requires the definition of the jump operators (Lindblad operators). In this manuscript we consider two different cases. The first type of jumps we analyze is the one that lead to the global Symmetry-Preserving Dissipation (SPD) dynamics [6]. The jump operators are defined as:

$$\hat{L}_i = \begin{cases} \hat{L}_{j,A} = \sqrt{\gamma_j} \hat{c}_{j,A}, \\ \hat{L}_{j,B} = \sqrt{\gamma_j} \hat{c}_{j,B}^\dagger, \end{cases} \quad (7)$$

In Eq. (7) we assumed that the associated dissipation

strength γ_j can be site-dependent since we will also study how jumps impact topological edge states and for this it is convenient to consider non-homogenous coupling to the external environment. The non-Hermitian Hamiltonian associated to this dynamics (no-jump trajectory) has been first theoretically proposed in Ref. [62] and then experimentally implemented [63] in a photonic lattice with engineered gain and loss, and robust topological edge states have been observed. We sketch this dissipation in Fig. 1(b) emphasizing that in each cell there is one site where fermions are injected by the Lindbladian, and the other where fermions leak out, with the same rate.

The second type of jump operators that we will analyze corresponds to the Lindbladian with global Symmetry-Breaking Dissipation (SBD) [6],

$$\hat{L}_i = \begin{cases} \hat{L}_{j,A} = \sqrt{\gamma_j} (\hat{c}_{j,A} + \hat{c}_{j,B}) , \\ \hat{L}_{j,B} = \sqrt{\gamma_j} (\hat{c}_{j,B} + \hat{c}_{j+1,A}) . \end{cases} \quad (8)$$

Fig. 1(c) shows that each Lindblad operator acts on pairs of sites and has the effect of losses, that is, fermions leak out of the system. Jump operators in Eq. (7) and Eq. (8) lead to a Lindblad dynamics that respectively satisfies/breaks the generalized symmetry relations that characterize the BDI class in presence of dissipation, as proposed in Ref. [6]. Further details about this topological classification of dissipators (the so-called dissipative tenfold way) are provided in Appendix B.

As briefly mentioned above, in order to assess the impact of dissipation on the edge modes, we will consider the possibility that the jump operators involve only a portion of $\lfloor \alpha L \rfloor$ ($\lfloor \cdot \rfloor$ is the floor function) central sites, with $\alpha \in [0, 1]$ such that, once we fix the parameters of the system and the range of lengths we will deal with, the edges of the chain are left untouched. This can be achieved by adjusting the site-dependent values of $\gamma_{j,A/B}$ so that they are different from zero on a limited portion of central sites. We have numerically verified that choosing $\alpha = 0.8$ is sufficient to separate the bulk dissipation from the boundary. Fig. 1(a) is a sketch representing how the zero-energy modes are exponentially localized at the edges of the chain in such a way that a non-homogeneous SPD or SBD environment with a suitable choice of α might not touch them.

The Lindbladian that we take into account is quadratic, since the Hamiltonian of the SSH model is quadratic and the jump operators are linear in the fermionic operators. Given a Gaussian state as initial condition of a quadratic dissipative dynamics, its Gaussian character is preserved in time, so that Wick's theorem holds for its whole evolution in time (see Appendix C for more details on Gaussian states).

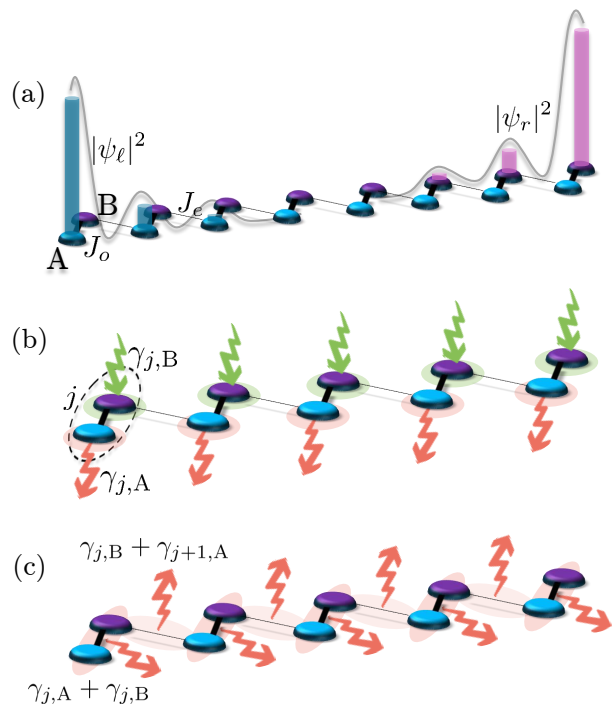


FIG. 1: (a) Sketch of the probability amplitude of the zero-mode states $|\psi_\ell\rangle$ and $|\psi_r\rangle$ that are exponentially localized at the edges of the SSH chain. (b) Sketch of the symmetry-preserving environment. The dotted oval represents the j -th unit cell. The green and orange shaded shapes represent the sites involved by the single Lindblad operators. (c) Sketch of the symmetry-breaking environment.

III. DISCONNECTED ENTANGLEMENT ENTROPY ALONG QUANTUM TRAJECTORIES

Having defined the model and its dynamics, we now discuss the quantity that we will use to study the dynamics of edge modes, the DEE, employed for quantum quenches in Refs. [49–51].

Let us consider a connected bipartition of a system into two subsets X and \bar{X} . The von Neumann bipartite entanglement entropy of the subsystem in X is defined as

$$S_X = -\text{Tr}_X (\hat{\rho}_X \log_2 \hat{\rho}_X), \quad (9)$$

where $\hat{\rho}_X = \text{Tr}_{\bar{X}} \hat{\rho}$ is the reduced density matrix of the system in X and $\{\lambda\}$ is the set of its eigenvalues and $\hat{\rho}$ is a pure state. By choosing the different bi-partitions as shown in Fig. 2, the DEE is defined as [64]

$$S^D = S_A + S_B - S_{A \cup B} - S_{A \cap B}. \quad (10)$$

The DEE is able to detect the presence of edge modes, thus being equal to 2 in the topological phase or to 0 in the trivial phase for the SSH chain. A disconnected

partition is necessary for the definition of a marker of topological phases since the entanglement spectrum of single connected partitions is not able to distinguish the topological character of wave functions [49]. A more detailed explanation of the properties of DEE is provided in Appendix A.

For Gaussian states, computing the entanglement entropy for a subset X of a partition is equivalent to computing the spectrum $\{\zeta\}$ of the reduced covariance matrix $\mathbf{G}^{(\text{traj})}$ of the same subsystem. The elements of this covariance matrix are

$$\mathbf{G}_{i,i'}^{(\text{traj})} = \langle \psi(t) | \hat{c}_i^\dagger \hat{c}_{i'} | \psi(t) \rangle = \text{Tr}(\hat{\rho}_x \hat{c}_i^\dagger \hat{c}_{i'}), \quad (11)$$

where $i, i' \in X$ [65] and $|\psi(t)\rangle$ is the state along the considered quantum trajectory.

Since the dissipative dynamics is quadratic, hence preserving the Gaussian character of the initial state, we directly evolve the covariance matrix of the reduced system (11) on each single trajectory. Details on the calculations are provided in Appendix D and in Appendix E. Resorting to the properties of free fermions (Appendix C), we obtain $S^{(D, \text{traj})}$, and we can analyze its statistical properties because it is a stochastic variable itself. In particular, we can compute its expected value averaging over trajectories

$$S^D = \overline{S^{(D, \text{traj})}},$$

as well as the probability distribution function of its variations under quantum jumps $P(\Delta S^D)$, evaluated over time and trajectories (see Sec. IV.3).

IV. RESULTS

In this section, we investigate the stability of the topological phase under dissipation by evaluating the DEE along quantum trajectories.

In order to get a first insight on the impact of Lindblad dynamics on the edge states, we first discuss the spreading of the edge modes due to dissipation. Next, we investigate the time-evolution of the expectation value of

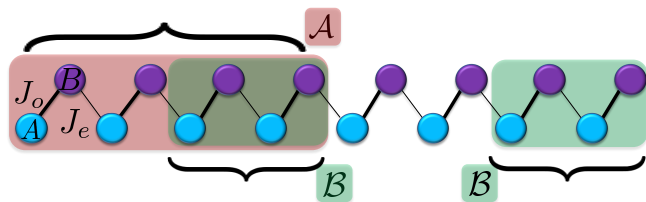


FIG. 2: Disconnected partition of the SSH chain. The red connected subset is named \mathcal{A} , while the green disconnected one is named \mathcal{B} . The blue (odd) sites represent the sublattice indices A , while the purple (even) sites represent the sublattice indices B . J_o and J_e are the intra-cell and inter-cell hopping amplitudes, respectively.

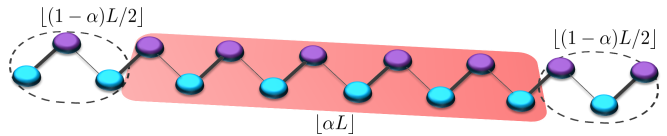


FIG. 3: Range of the non-homogeneous SPD dissipation. When $[\alpha L]$ central sites are affected by dissipation, there are $n = [(1-\alpha)L/2]$ sites left of each edge on the chain.

the DEE under the two types of dissipation — SPD and SBD — outlined in the previous sections.

IV.1. Spreading of the edge modes

The existence of edge states is a well-known characteristics of topological insulators under open boundary conditions. The localization of the edge modes depends on the choice of the ratio J_o/J_e and on the length of the chain [56]. In the limit of perfectly dimerized chain, as shown in Appendix A, the edge modes are exactly localized at the two edge sites. On the contrary, when $J_o/J_e > 0$, the modes have an exponential decay within the bulk of the chain. As a consequence, owing to the long-range entanglement, the existence of a non-zero correlation among the edge sites of the chain can also characterize a topological state. For instance, the topological order would be disrupted if the boundary modes vanish under the action of a dissipation, and this would be probed by the correlations going to zero as well.

For this reason, we look at the time evolution of the covariance matrix

$$\mathbf{G} = \overline{\mathbf{G}^{(\text{traj})}},$$

averaged over trajectories (the covariance matrix is a linear function of the state and its average over trajectories coincides with its evaluation using the density matrix).

Not surprisingly, not all the quantum-jump protocols have the same effect on the edge modes. To show this, we consider a site-dependent decay rate. This non-homogeneous dissipation leaves $n = \lfloor \frac{L(1-\alpha)}{2} \rfloor$ sites untouched near each edge, as shown in Fig. 3. Defining ξ as the characteristic localization length of the edge modes (see Appendix A for details), we study the evolution of the correlator $G_{1,L}(t)$ for different values of the ratio $\nu = n/\xi$.

In Fig. 4 we show the time evolution of $G_{1,L}$ for different values of α and ν at fixed J_o/J_e and size L of the chain. The initial correlation between the two edge modes is lost with time. The time scale over which this happens depends strongly on ν , the larger is the number of boundary sites not touched by dissipation, the slower the suppression of the correlation occurs.

For α small enough so that $n \gg \xi$, the Lindblad operators act sufficiently far from the range where the edge

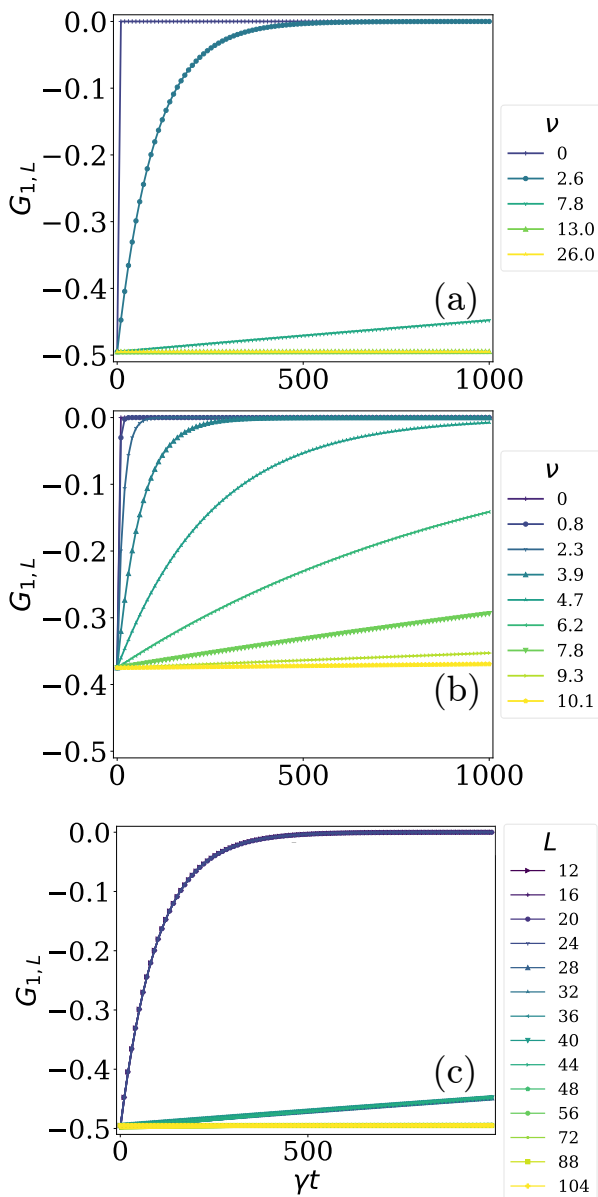


FIG. 4: Two-point correlator for the α -SPD dynamics for $L = 112$ and different values of α decreases. For decreasing α a growing fraction $\nu = \frac{(1-\alpha)L}{2\xi}$ of sites near each edge is left untouched. The system is initialized in the topological half-filled ground state of the Hamiltonian of the isolated SSH chain with parameters $J_o/J_e = 0.1$ — for which $\xi = 0.43$ — in Panel (a) and $J_o/J_e = 0.5$ — for which $\xi = 1.44$ — in Panel (b), with $N = 56$ unit cells ($L = 112$ sites). In Panel (c) α is fixed at 0.8 and L is varied. The system is initialized with $J_o/J_e = 0.1$.

modes at $t = 0$ are localized, in this case the correlation is very weakly dependent on time and correlations are preserved [see Figs. 4(a,b)]. This behavior does not depend on the particular type of dissipation considered.

In this case, we can safely conclude that for values of $\alpha \approx 0.8$ the boundaries are unaffected by dissipation.

In Fig. 4(c), we present the time evolution of the two-point correlator for different system sizes, having fixed $\alpha = 0.8$. The plot shows that by selecting an appropriate value of α , a sufficient number of sites remain unaffected by dissipation, allowing us to observe a decay in the two-point correlator over time, yet with significantly large decay times. For large enough system size, the correlator can be considered effectively constant within the timescales of interest. This result highlights a key distinction: while the introduction of a uniform dissipation drastically alters the correlation properties of the original topological system, carefully confining dissipation to the central region of the chain allows us to recover the same behavior observed in the unitary case, where correlations remain stable in time in the thermodynamic limit.

This preliminary analysis gives the flavor of the dynamics of the edge modes following a quench and evolving under the effect of dissipation. How does the dynamics of correlations between the edge modes reflect in the properties of the disconnected entanglement entropy? Being a nonlinear function of the state, it will contain additional information compared to those encoded in the density matrix.

IV.2. Time-evolution of the disconnected entanglement entropy

In Ref. [50], it has been shown that, in the case of a local, unitary ($\gamma = 0$) and symmetry-preserving quench, the time at which the DEE deviates from 2 (the initial state being in the topological phase) scales linearly with the system size, proving that the DEE is a good non-local order parameter for isolated topological systems in the thermodynamic limit.

Our aim is to extend this study to the dissipative case. Adopting the techniques described in Appendix C, we calculate the time evolution of the reduced covariance matrix for the subsystems \mathcal{A} , \mathcal{B} , $\mathcal{A} \cup \mathcal{B}$, and $\mathcal{A} \cap \mathcal{B}$ for a single trajectory. From the diagonalization of the reduced covariance matrix, we calculate the different contributions needed to evaluate the DEE. We average the result over multiple trajectories ($N_{\text{traj}} = 960$), calculating the error as the standard error. In the following, in Fig. 5 and Fig. 6, we show the time evolution of the DEE for $\alpha = 1$ (uniform) and $\alpha = 0.8$. In both cases, we consider growing system sizes.

We set the initial state of the dynamics as the ground state of the SSH chain in the topological phase, with an initial DEE value of 2. Our goal is to explore how the dynamics of the DEE changes when its evolution is governed not by a Hamiltonian inducing a unitary quench but by a Lindbladian. For brevity, in the following, we will refer to a topological (trivial) Hamiltonian as one whose parameters are chosen to ensure a topological (trivial) ground state.

Figs. 5 and 6 illustrate the impact of dissipation on the stability of the entangled topological edge modes for $\alpha =$

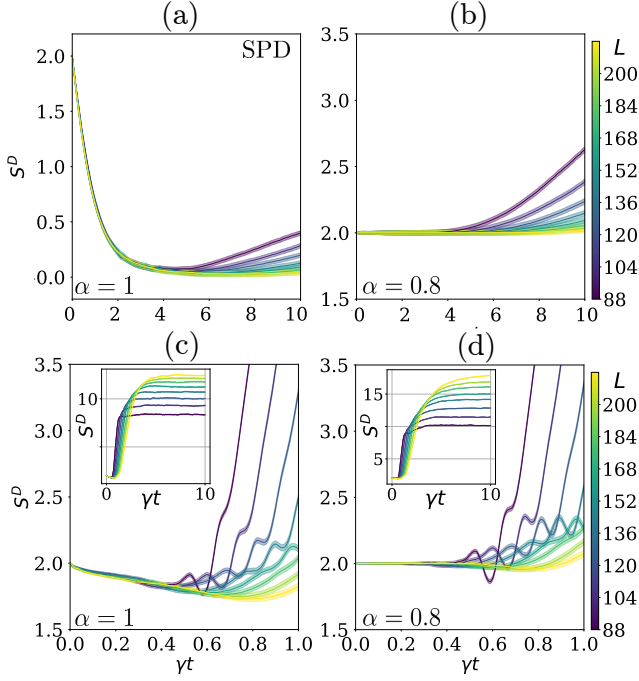


FIG. 5: Dynamics of the DEE under the SPD dynamics with $\gamma = 1$, $J_e/\gamma = 20$ until $\gamma t = 10.0$. (a) SPD with $\alpha = 1$ and topological Hamiltonian ($J_o/J_e = 0.1$), (b) SPD with $\alpha = 0.8$ and topological Hamiltonian ($J_o/J_e = 0.1$). (c) SPD with $\alpha = 1$ and trivial Hamiltonian ($J_o/J_e = 1.5$) until $\gamma t = 1.0$. (d) SPD with $\alpha = 0.8$ and trivial Hamiltonian ($J_o/J_e = 1.5$) until $\gamma t = 1.0$. (c,d) Inset plots: whole dynamics until $\gamma t = 10.0$.

1 [panels (a, c)] and $\alpha = 0.8$ [panels (b, d)]. Fig. 5 shows the results for the first type of dynamics (SPD), while Fig. 6 presents the same analysis for the second type (SBD). Among all pairs of panels with the same letter in the two figures, we observe clear similarities, leading us to conclude that there are no substantial differences between the two types of dissipation in terms of their impact on the properties of the average DEE.

In particular, in panels (a) of both figures, where the Hamiltonian governing the dynamics is topological and $\alpha = 1$, meaning that the dissipation is homogeneous, the DEE initially starts at 2 but quickly deviates from this value as time progresses. This variation is a direct consequence of dissipation — whether strictly local (SPD) or localized between two nearest-neighbor sites (SBD) — which tends to destroy entanglement both at short range (within the bulk) and, more significantly, at long range (between the two topological modes). Since the DEE detects only the latter, the observed variations in the plots are entirely due to the destruction of long-range topological entanglement. This behavior can be intuitively understood in the fully-dimerized limit of the chain and will be further analyzed in subsequent sections and in Appendix F.

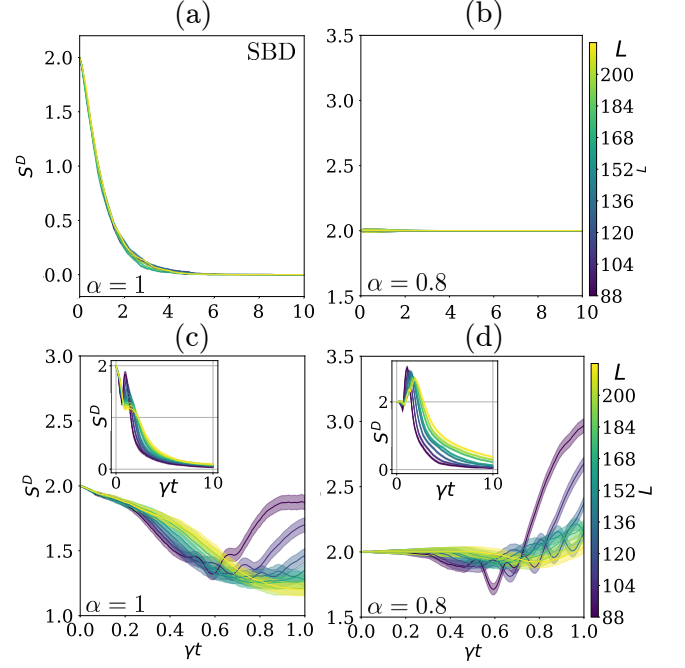


FIG. 6: Dynamics of the DEE under the SBD dynamics with $\gamma = 1$, $J_e/\gamma = 20$ until $\gamma t = 10.0$. (a) SBD with $\alpha = 1$ and topological Hamiltonian ($J_o/J_e = 0.1$), (b) SBD with $\alpha = 0.8$ and topological Hamiltonian ($J_o/J_e = 0.1$). (c) SBD with $\alpha = 1$ and trivial Hamiltonian ($J_o/J_e = 1.5$) until $\gamma t = 1.0$. (d) SBD with $\alpha = 0.8$ and trivial Hamiltonian ($J_o/J_e = 1.5$) until $\gamma t = 1.0$. (c,d) Inset plots: whole dynamics until $\gamma t = 10.0$.

In these cases, since the initial state is the half-filled ground state of the topological Hamiltonian and the coherent part of the Lindbladian coincides with the topological Hamiltonian, no quench contribution is present to counteract the measurement effects of the environment manifested through quantum jumps. As a result, quantum jumps dominate the dynamics, causing the DEE to steadily decrease to zero. However, while in the SBD case — where dissipation eventually depletes the entire chain — this value remains asymptotic, in the SPD case, the curves exhibit a recovery over a timescale that increases with system size. Since our focus is not on asymptotic entanglement properties, we do not investigate this scaling further.

Conversely, in panels (b), where $\alpha = 0.8$, effectively isolating the edges from dissipation, the behavior of the DEE changes drastically. Here, the DEE remains at 2, either persistently in the SBD case or for a time that scales linearly with system size in the SPD case, ensuring stability in the thermodynamic limit. The key difference between the $\alpha = 1$ and $\alpha = 0.8$ cases is that, in the latter, the edge modes remain unaffected by dissipation. Given that dissipation is spatially localized in both cases, this is sufficient to preserve the topological entanglement

associated with the edge modes.

Panels (c) introduce a crucial difference: here, the coherent part of the Lindbladian includes a trivial Hamiltonian, leading to a coherent quench contribution that competes with the dissipative effects dominating panels (a) and (b). This additional contribution partially mitigates the destructive impact of quantum jumps in the early stages of evolution, resulting in a behavior resembling a plateau. Strictly speaking, we use the term *plateau* to draw an analogy with the well-known unitary case, where the plateau corresponds to an initial segment with zero slope. In our case, however, it refers to an initial portion of the curve with a less pronounced slope compared to panels (a). Viewing these curves as tilted plateaus, we can interpret them as a meaningful generalization of the DEE dynamics observed in the unitary case (see Ref. [50]). In the unitary limit, the DEE remains equal to 2 for a time that scales linearly with system size. Here, we define a critical time beyond which the tilted plateau disappears and analyze its deviation from the unitary scenario. In these and in panels (d) we show the inset plots with the whole dynamics until the curves reach an asymptotic value. However, again, we do not investigate further the asymptotic properties of the DEE.

Finally, panels (d) reveal another intriguing result: Even when the coherent part of the Lindbladian corresponds to a trivial Hamiltonian, the DEE remains robust as long as the edges of the chain are protected. This confirms that, since long-range entanglement is encoded in the occupation number basis of the fermionic edge modes, local dissipation inevitably destroys it. The only way to preserve robustness, as in the unitary case, is to shield the edges from dissipation. Once this protection is in place, the DEE remains stable regardless of the coherent part of the Lindbladian dynamics, mirroring the unitary case where stability under symmetry-preserving quenches was demonstrated [50].

On the other hand, when dissipation affects the edges, the coherent part of the Lindbladian becomes crucial in determining the DEE's robustness. Within a single trajectory, the dynamic contributions from quantum jumps and those from the non-Hermitian Hamiltonian component compete with each other [57]. As a result, introducing a quench with a trivial Hamiltonian enhances stability, as the destructive effect of quantum jumps is mitigated in the initial stages of DEE evolution.

As already mentioned, in the time traces of Fig. 5 and 6 the DEE departs from the initial (topological) value at a given time scale. In the numerics, we estimate it in the following way: for each trajectory, we evaluate $\gamma t_c^{(\text{traj})}$ as the first time at which the threshold condition $|S^{(D,\text{traj})}(t) - S^{(D,\text{traj})}(0)| < (2 \log_2 2)/100$ is met. We then average it $\gamma t_c = \overline{\gamma t_c^{(\text{traj})}}$ over trajectories. We have checked that different threshold levels provide qualitatively similar results. Fig. 7 shows γt_c versus L for the case of $\alpha = 0.8$ SPD dissipation and topological Hamil-

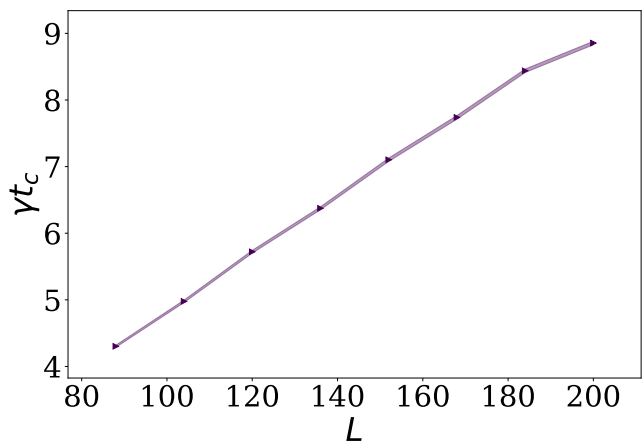


FIG. 7: Linear scaling of γt_c as function of L corresponding to the curves of Fig. 5(b). Non-homogeneous SPD dissipation and topological Hamiltonian driving the evolution with $J_o/J_e = 0.1$, $\alpha = 0.8$, $\gamma = 1$, and $J_e/\gamma = 20$.

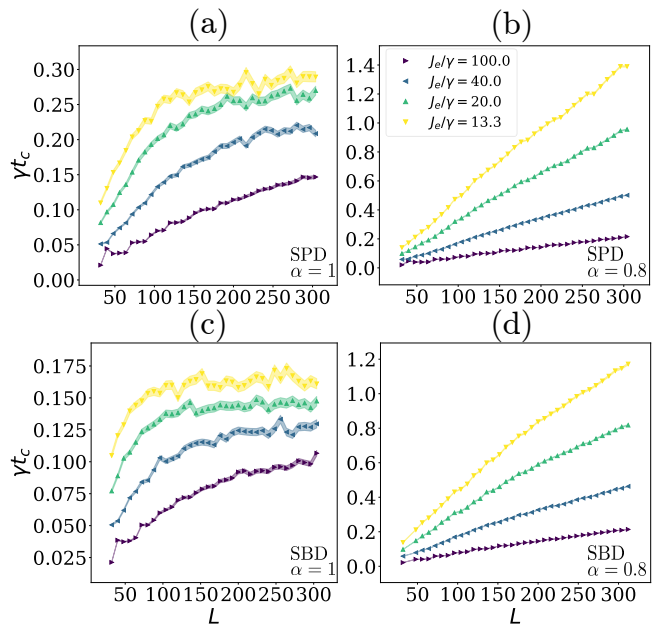


FIG. 8: γt_c versus L with various choices of J_e/γ . (a) SPD dynamics with $\alpha = 1$. (b) SPD dynamics with $\alpha = 0.8$. (c) SBD dynamics with $\alpha = 1$. (d) SBD dynamics with $\alpha = 0.8$. Trivial Hamiltonian ($J_o/J_e = 1.5$), $\gamma = 1$, and $J_e/\gamma = 20$.

tonian driving the evolution [see Fig. 5(b)]. We see that t_c linearly increases with L and this shows that when the quantum jumps do not involve the edges of the chain, the DEE remains quantized in the thermodynamic limit.

Fig. 8 shows how γt_c scales with the system size for the three dynamics with the trivial Hamiltonian, namely corresponding to the curves of Figs. 5(c), 5(d), 6(c) and 6(d). The analysis of the characteristic time γt_c , shown

in Fig 8, reveals distinct scaling behaviors depending on the dissipation profile. When $\alpha = 0.8$ [Fig. 8(b,d)], the dissipation is confined to the bulk and γt_c increases linearly with system size, indicating that the entangled edge states remain stable for increasingly long times. This scaling matches what is observed in the unitary case, where topological edge modes persist indefinitely in the thermodynamic limit. However, when $\alpha = 1$ [Fig. 8(a,c)], the dissipation acts on the boundaries and γt_c saturates at a finite value, signaling that the entanglement between the edge modes is eventually lost after a finite time, regardless of system size. This marks a crucial difference from the unitary scenario, where the DEE deviation time scales linearly and indefinitely with size. Here, instead, the presence of dissipation at the edges imposes a strict limit on the survival of the topological correlations, leading to their complete suppression within a finite timescale. However, again, imposing $\alpha < 1$, provides results similar to those of the unitary case.

In summary, when examining the time evolution of the DEE starting from a topological state, the action of the dissipation on the boundary appears to be the most relevant aspect to consider. On the contrary, belonging to one class rather than another within the tenfold way framework appears to have no significant relevance in the study of the time evolution of the DEE. In the next section we inquire more deeply this fact by looking at the changes in DEE due to the effect of quantum jumps.

IV.3. Time-resolved statistics of ΔS^D

To gain a deeper understanding of how the DEE evolves along individual quantum trajectories, we analyze the statistical distribution of its variations due to quantum jumps. The typical pattern consists of an evolution driven by the non-Hermitian Hamiltonian, abruptly interrupted by a discontinuous change in entanglement entropy at the occurrence of a jump. These changes, which can either increase ($\Delta S^D > 0$) or decrease ($\Delta S^D < 0$) the DEE, are illustrated in Fig. 9 [57]. To systematically characterize this behavior, we sample the changes in entanglement entropy at each jump event along a trajectory and repeat this process over multiple realizations to construct the histogram $P(\Delta S^D)$. The aim is to identify whether the variations follow a structured pattern and to determine whether specific jump events are responsible for significant entanglement loss.

Figure 10 presents the statistical analysis for the two homogeneous dissipative dynamics, namely with $\alpha = 1$. We consider a system of $L = 56$ sites with the topological Hamiltonian as the coherent contribution. The average dynamics generated by Eq. (1) under these conditions allows us to distinguish two different time windows — an initial transient regime, and a later stage where the DEE approaches its stationary value. We perform a statistical analysis of these windows separately. More precisely, in the SBD case, we show only the statistical analysis re-

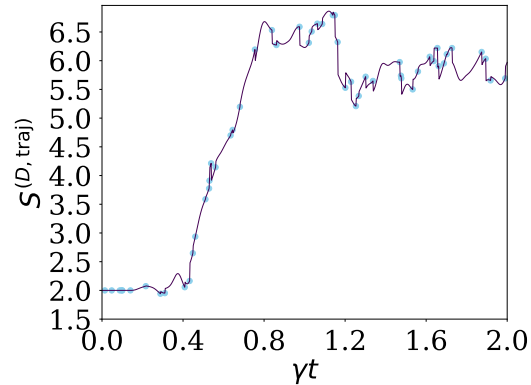


FIG. 9: Time evolution of the DEE over a single trajectory, namely $S^{(D, \text{traj})}$. The blue dots correspond to the occurrence of a quantum jump on any site apart from the two edges, where the occurrence of the jump is signaled by a blue dot.

lated to the first time window, because later the chain is emptied by dissipation and no more jumps occur.

As shown in Fig. 10, the distribution of ΔS^D reveals distinct signatures depending on the type of dissipation. In the SPD case [Fig. 10(a)], the early stage shows a bimodal distribution with a pronounced peak at $\Delta S^D = -2$, signaling the destruction of topological entanglement. In the later stage [Fig. 10(b)], this peak disappears and the distribution becomes unimodal, indicating that the destruction of entanglement has already occurred. In contrast, the SBD case [Fig. 10(c)] exhibits a similar peak at $\Delta S^D = -2$, but an additional peak at $\Delta S^D = \Delta S^D = 2 - 2(-\frac{3}{4} \log_2(3) + 2) \approx -0.38$ (signaled by a yellow circle) emerges, which can be attributed to the extended nature of the jump operators in this dissipation model. We will further analyze it in Appendix F.

To further investigate the role of spatially localized dissipation, we analyze the SPD case that does not affect the edges, i.e., with $\alpha = 0.8$, shown in Fig. 11. In this case, where dissipation is confined to the central region of the chain, the distributions remain unimodal at all times. The absence of the $\Delta S^D = -2$ peak confirms that the edge states are unaffected by the quantum jumps. This result strongly suggests that the entanglement between boundary modes is disrupted only when the dissipation acts directly on the edges.

A key observation is that the pronounced peaks observed in the homogeneous dissipation cases indicate that the effect of quantum jumps on the DEE manifests in a discrete manner for the SPD dynamics. This suggests that when a quantum jump is localized on one of the two edge sites, the entanglement entropy undergoes an abrupt and quantized reduction, particularly in the early transient regime. To further confirm this interpretation, we perform a site-resolved analysis of ΔS^D to explicitly verify whether jumps occurring at the boundary sites are

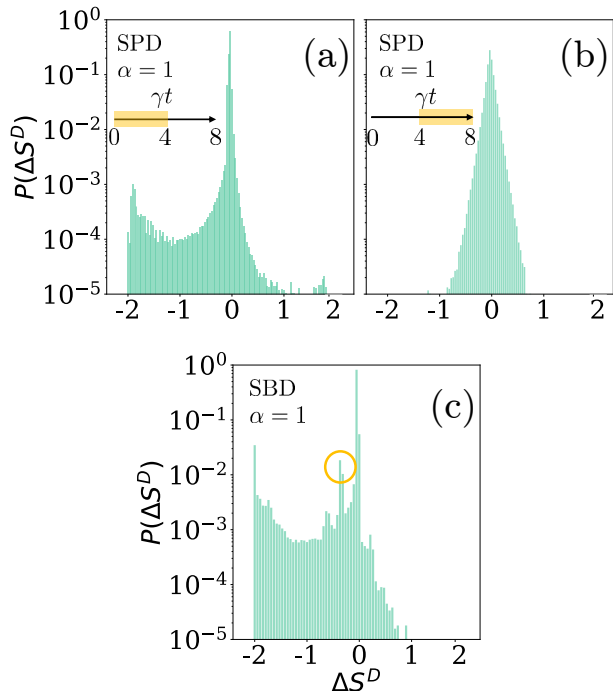


FIG. 10: $P(\Delta S^D)$ for the two different time windows of the two homogeneous dynamics. (a) SPD with $\alpha = 1$, $t_0 = 0.0$, $t_f = 4.0$ (yellow highlighted time interval). (b) SPD with $\alpha = 1$, $t_0 = 4.0$, $t_f = 8.0$ (yellow highlighted time interval). (c) SBD with $\alpha = 1$, $t_0 = 0.0$, $t_f = 4.0$. We do not show the statistical analysis related to the second time window for the global SBD dynamics since the chain is emptied by dissipation and no more jumps occur. The initial state is the ground state of \hat{H}_{SSH} with $L = 56$ sites, $J_o/J_e = 0.1$ and the parameters of the dissipative evolution are $\gamma = 1$, $J_o/J_e = 0.1$, $J_e/\gamma = 20$ and $N_{\text{traj}} = 28800$ trajectories. The yellow circle signals the peak at $\Delta S^D = \Delta S^D = 2 - 2(-\frac{3}{4} \log_2(3) + 2) \approx -0.38$.

responsible for these discrete entanglement changes.

IV.4. Site-resolved statistics of ΔS^D

The analysis of the time-resolved statistics of ΔS^D in the previous section revealed the presence of distinct peaks, particularly at $\Delta S^D = -2$ for the homogeneous ($\alpha = 1$) SPD dynamics, suggesting that specific quantum jumps play a dominant role in destroying topological entanglement. To verify whether these critical jumps occur at specific sites in the chain, we now investigate the site-resolved distribution of ΔS^D .

Since the characteristic peaks in $P(\Delta S^D)$ appear primarily in the first time window of the SPD and SBD homogeneous dissipations ($\alpha = 1$), we focus on this interval. For each trajectory, we record the site index j

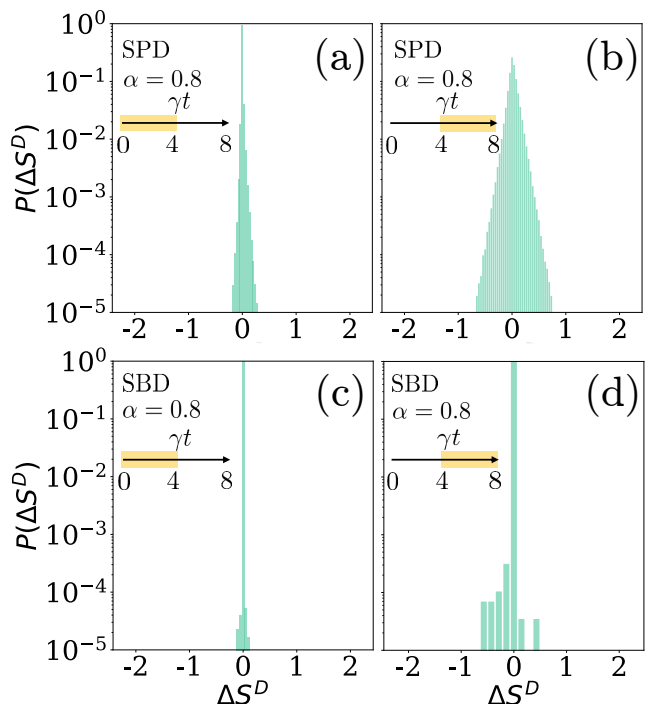


FIG. 11: $P(\Delta S^D)$ for the two different time windows of the SPD dynamics with $\alpha = 0.8$. (a) SPD, $t_0 = 0.0$, $t_f = 4.0$. (b) SPD, $t_0 = 4.0$, $t_f = 8.0$. (c) SBD, $t_0 = 0.0$, $t_f = 4.0$. (d) SBD, $t_0 = 4.0$, $t_f = 8.0$.

where the jump leading to a ΔS^D occurs and analyze the conditional probability distribution $P_j(\Delta S^D)$ for different sites. Figure 12(a) shows the site-resolved histogram for the SPD dynamics with $\alpha = 1$. We observe that the peak at ΔS^D is exclusively associated with jumps occurring at the boundary sites ($j = 1$). This result strongly supports our previous hypothesis — the destruction of topological entanglement occurs due to quantum jumps acting directly on the edge modes, where their Bell-pair entanglement is lost. Furthermore, the data suggest that the first jump occurring at the boundary site in each trajectory contributes predominantly to this peak, as further discussed in Appendix F.

In contrast, for the SBD case with $\alpha = 1$ shown in Fig. 12(b), while a peak at $\Delta S^D = -2$ is still observed for boundary jumps, an additional peak emerges at $\Delta S^D \approx -0.38$. This secondary peak originates from the non-local nature of the SBD jump operators, which affect entanglement more gradually rather than in a single discrete step. As demonstrated in Appendix F, the first jump does not immediately destroy the boundary entanglement but instead leads to a partial entanglement reduction, reflected in the peak at $\Delta S^D \approx -0.38$. The later jumps at the boundaries eventually lead to the complete destruction of the edge modes, giving rise to the $\Delta S^D = -2$ peak.

Overall, this site-resolved analysis confirms that, in the SPD case, the loss of topological entanglement occurs in

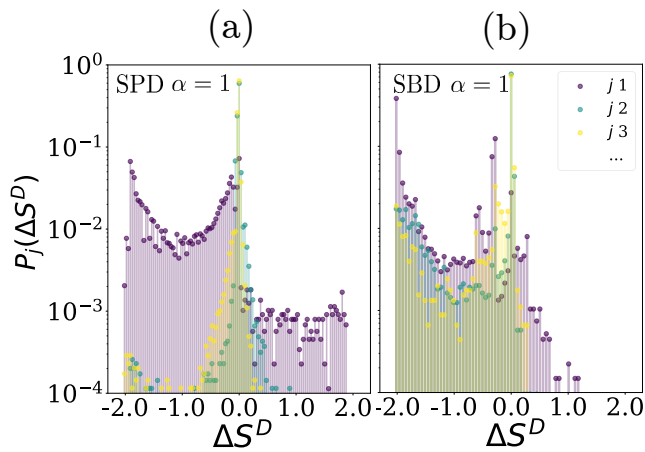


FIG. 12: $P(\Delta S^D)$ conditioned on the site where the jump has occurred. (a) SPD with $\alpha = 1$. (b) SBD with $\alpha = 1$. We focus the statistical analysis in the first time window going from $\gamma t_0 = 0.0$ to $\gamma t_f = 4.0$. The statistical analysis is done considering a sample of $N_{\text{traj}} = 28800$ trajectories.

a discrete manner — a single jump at the boundary is sufficient to destroy the edge modes, producing a sharp and quantized change in the DEE. This result highlights a key difference from the SBD case, where the effect of quantum jumps is more gradual due to the extended nature of the dissipation process.

V. DISCUSSION AND CONCLUSIONS

In this manuscript, we explored the topological properties of the monitored Su-Schrieffer-Heeger model, our focus being on how monitored dynamics can provide insights into topology in open quantum systems. By employing the quantum jump approach, we accessed to non-linear functions of the quantum state, revealing aspects of topological behavior that may be hidden in a density matrix formulation.

The central quantity we analyzed is the Disconnected Entanglement Entropy, averaged over trajectories, and studied the evolution of this average under different types of couplings to the environment (i.e. different types of quantum jumps). Furthermore, we also examined the discrete changes in the DEE induced by individual quantum jumps (in particular, we also considered time-resolved statistics, distinguishing between the early and late stages of the evolution).

Summarizing:

- By analyzing the evolution of the average DEE, we showed that the effects of dissipation are primarily governed by its spatial arrangement rather than its symmetry classification within the tenfold way framework. When dissipation extends homogeneously throughout the chain, the coherent con-

tribution to the dynamics becomes crucial in determining the robustness of the DEE, that anyway deviates from its topological value after a finite time. Conversely, when dissipation is restricted to the central region of the chain, the entangled edge states remain stable for a time that scales linearly with system size, regardless of the coherent dynamical contribution. This finding aligns with previous works on the unitary dynamics of topological systems and demonstrates that edge states can be protected from decoherence as long as boundary dissipation is avoided.

- Through the statistical analysis of quantum jumps, we revealed that boundary jumps play a dominant role in the destruction of topological order. Sometimes — when they are local — they lead to discrete changes in the DEE associated with the sudden loss of the topological long-range entangled Bell pair.

Furthermore, our results reinforce the conclusions of previous works [6], suggesting that the tenfold way classification for quadratic Lindbladians is insufficient for predicting the dynamical properties of open systems. While this classification provides insight into the single-particle spectrum of the Lindbladian, it does not capture the evolution of entanglement properties or the stability of edge modes under dissipation. A similar result has been observed in the unitary case, where topological and non-topological Hamiltonians provide a similar evolution for the DEE [50].

ACKNOWLEDGMENTS

We would like to thank Dario Bercioux, Marcello Dalmonte, Sebastian Diehl, Gabriele Campagnano and Vittorio Vitale for very helpful discussions. G.P. acknowledges computational resources from the CINECA award under the ISCRA initiative, and from MUR, PON Ricerca e Innovazione 2014-2020, under Grant No. PIR01_00011 - (I.Bi.S.Co.). This work was supported by PNRR MUR project PE0000023 - NQSTI, by the European Union's Horizon 2020 research and innovation programme under Grant Agreement No 101017733, by the MUR project CN_00000013-ICSC (P.L.), by the MUR project PRIN 2022H77XB7 (G.E.S.), and by the QuantERA II Programme STAQS project that has received funding from the European Union's Horizon 2020 research and innovation programme under Grant Agreement No 101017733 (P.L. and G.E.S.). This work is co-funded by the European Union (ERC, RAVE, 101053159) (R.F.). Views and opinions expressed are however those of the authors only and do not necessarily reflect those of the European Union or the European Research Council. Neither the European Union nor the granting authority can be held responsible for them.

Appendix A: Details on the fully dimerized limit of the SSH chain and DEE

1. Edge modes

Considering the Hamiltonian of Eq. (6) with space-dependent couplings [56],

it is straightforward to see that, in the thermodynamic limit, two zero-energy eigenmodes of the Hamiltonian can be found in the form

$$|L\rangle = \sum_{i=1}^N a_i \hat{c}_{i,A}^\dagger |0\rangle = \sum_{i=1}^N a_i |i, A\rangle, \quad (\text{A1a})$$

$$|R\rangle = \sum_{i=1}^N b_i \hat{c}_{i,B}^\dagger |0\rangle = \sum_{i=1}^N b_i |i, B\rangle, \quad (\text{A1b})$$

which are states exponentially localized at either the first site A or the last site B of the chain. In (A1), the coefficients are given by

$$a_i = - \prod_{j=1}^{i-1} \frac{J_{oj}}{J_{ej}} a_1 \quad i = 2, \dots, N \quad (\text{A2a})$$

$$b_i = b_N \frac{-J_{oN}}{J_{ei}} \prod_{j=i+1}^{N-1} \frac{-J_{oj}}{J_{ej}} \quad i = 1, \dots, N-1 \quad (\text{A2b})$$

$$b_1 = a_N = 0. \quad (\text{A2c})$$

The condition Eq. (A2c) is instead incompatible with the existence of zero-energy modes and one must consider the small lift Δ — which is exponentially decaying in the system's size — in the degeneracy between the two edge states. The best approximations of the two edge states are thus the two orthogonal real equal-weighted superpositions of the two. This superposition generates an additional saturated contribution to the entanglement entropy of a partition that includes one edge without the second, like \mathcal{A} and \mathcal{B}/\mathcal{A} in Fig. 2. More precisely, in the fully dimerized topological limit, we can write

$$|L\rangle = \hat{c}_{1,A}^\dagger |0\rangle = |1_{1A} 0_{NB}\rangle \quad (\text{A3a})$$

$$|R\rangle = \hat{c}_{N,B}^\dagger |0\rangle = |0_{1A} 1_{NB}\rangle \quad (\text{A3b})$$

we can write the density matrix of the superposition (singlet) state as

$$\hat{\rho}_{\mathcal{AB}} = \frac{1}{2} [|1_{1A} 0_{NB}\rangle \langle 0_{NB} 1_{0A}| + |0_{1A} 1_{NB}\rangle \langle 1_{NB} 0_{1A}| + |1_{1A} 0_{NB}\rangle \langle 1_{NB} 0_{1A}| + |0_{1A} 1_{NB}\rangle \langle 0_{NB} 1_{1A}|]. \quad (\text{A4})$$

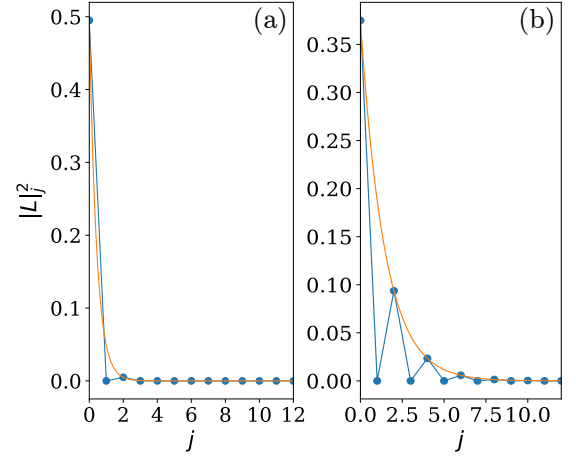


FIG. 13: Edge modes distribution for a topological Hamiltonian with (a) $J_o/J_e = 0.1$ (b) $J_o/J_e = 0.5$. Blue curve: probability amplitude. Orange curve: exponential fit $|L|_j^2 = e^{-j/\xi}$.

When the chain is not in the perfectly dimerized limit, the edge modes (specifically, their probability distribution $|L|_j^2$ or $|R|_j^2$) decay exponentially into the bulk as function of the site index j , as shown in Fig. 13 for the left edge mode, without loss of generality. By fitting an exponential function, we estimate the characteristic localization length ξ of the decay $|L|_j^2 = e^{-j/\xi}$, where j is the site index.

2. Disconnected entanglement entropy

It is thus possible to analytically understand the role of the DEE in the fully-dimerized and topological limit of the SSH chain and show that the ground state always contains the maximally entangled superposition of the two edge states in the topological phase. The reduced system is thus

$$\hat{\rho}_{\mathcal{B}} = \frac{1}{2} [|0_{NB}\rangle \langle 0_{NB}| + |1_{NB}\rangle \langle 1_{NB}|], \quad (\text{A5})$$

so that $S_{\mathcal{B}_{edge}} = S_{\mathcal{A}_{edge}} = \log_2 2$. This extra contribution is added to the other bulk contributions which depend on the cuts of the chosen partitions.

In the thermodynamic limit it can be easily shown [50] that the latter give a zero contribution, so that only the edge contribution survives and $\lim_{L \rightarrow \infty} S^D = 2 \log_2 2$. More generally, in the thermodynamic limit, the value of S^D is fixed by the number of edge states \mathcal{D} , which is in turn fixed by the bulk-boundary correspondence [66], i.e., $\lim_{L \rightarrow \infty} S^D = \log_2 \mathcal{D}$. For this reason, the DEE is said to correspond to the thermodynamic entropy at zero temperature of one edge [50].

Appendix B: Details on symmetry classifications for open systems

1. Nambu Formalism

Let \hat{c}_j be the destruction operator for a system of spinless fermions labelled by $j = 1, \dots, L$. We define a Nambu column vector $\hat{\mathbf{C}}$ and its Hermitian conjugate row vector $\hat{\mathbf{C}}^\dagger$, each of length $2L$, by [67]

$$\hat{\mathbf{C}} = \begin{pmatrix} \hat{c}_1 \\ \vdots \\ \hat{c}_L \\ \hat{c}_1^\dagger \\ \vdots \\ \hat{c}_L^\dagger \end{pmatrix}, \quad (\text{B1})$$

and

$$\hat{\mathbf{C}}^\dagger = (\hat{c}_1^\dagger, \dots, \hat{c}_L^\dagger, \hat{c}_1, \dots, \hat{c}_L). \quad (\text{B2})$$

Majorana fermions are Hermitian combinations of ordinary complex fermions:

$$\check{\mathbf{c}} = \begin{pmatrix} \check{\mathbf{c}}_1 \\ \check{\mathbf{c}}_2 \end{pmatrix}, \quad (\text{B3})$$

where $\check{\mathbf{c}}_1$ and $\check{\mathbf{c}}_2$ are L -dimensional (column) vectors whose elements are:

$$\check{c}_{1,j} = (\hat{c}_j^\dagger + \hat{c}_j) \quad \text{and} \quad \check{c}_{2,j} = i(\hat{c}_j^\dagger - \hat{c}_j). \quad (\text{B4})$$

These operators are manifestly Hermitian. They allow us to express the original fermions as:

$$\hat{c}_j = \frac{1}{2}(\check{c}_{1,j} + i\check{c}_{2,j}) \quad \text{and} \quad \hat{c}_j^\dagger = \frac{1}{2}(\check{c}_{1,j} - i\check{c}_{2,j}), \quad (\text{B5})$$

and satisfy the anti-commutation relations:

$$\{\check{c}_{\alpha,j}, \check{c}_{\alpha',j'}\} = 2\delta_{\alpha,\alpha'}\delta_{j,j'}. \quad (\text{B6})$$

To be consistent with the Nambu notation for the ordinary fermions, we better define the Majorana column vector [68]:

$$\check{\mathbf{c}} = \mathbf{W}\hat{\mathbf{C}}, \quad (\text{B7})$$

where we defined the $2L \times 2L$ block matrix:

$$\mathbf{W} = \begin{pmatrix} \mathbf{1} & \mathbf{1} \\ -i\mathbf{1} & i\mathbf{1} \end{pmatrix} \quad \text{such that} \quad \mathbf{W}\mathbf{W}^\dagger = \mathbf{W}^\dagger\mathbf{W} = 2\mathbf{1}. \quad (\text{B8})$$

2. Symmetry classes for open systems: review of the tenfold way classification of quadratic Lindbladians

We review the symmetry classification for quadratic open Markovian systems proposed in Ref. [6]. We start

by writing the quadratic Hamiltonian in Eq. (6) and the linear jump operators in terms of the $2L$ Majorana operators $\{\check{c}_j\}$ defined in Eq. (B5) such that

$$\hat{H}_{\text{SSH}} = \sum_{j,j'=1}^{2L} \check{c}_j \mathbf{H}_{j,j'}^M \check{c}_{j'}, \quad (\text{B9a})$$

$$\hat{L}_\mu = \sum_{j=1}^{2L} \ell_{\mu j} \check{c}_j, \quad (\text{B9b})$$

where $\mathbf{H}_{j,j'}^M$ are the matrix elements of a $2L \times 2L$ matrix \mathbf{H}^M which is purely imaginary and anti-symmetric, $\mathbf{H}^{M^\text{T}} = -\mathbf{H}^M$, while $\ell_{\mu j} \in \mathbb{C}$. The superscript in \mathbf{H}^M underlines the fact that the Hamiltonian is written in the Majorana operators basis. The dissipation is encoded into a $2L \times 2L$ complex (semi)-positive definite Hermitian matrix \mathbf{M} whose elements are $M_{j,j'} = \sum_\mu \ell_{\mu j} \ell_{\mu j'}^*$. Since $\mathbf{M}^* = \mathbf{M}^\text{T}$, the real part of \mathbf{M} , $\mathbf{M}_\text{R} = \frac{1}{2}(\mathbf{M} + \mathbf{M}^*)$, is a (semi)-positive definite symmetric matrix, while the imaginary part, $\mathbf{M}_\text{I} = \frac{1}{2i}(\mathbf{M} - \mathbf{M}^*)$, is anti-symmetric. (One can show that \mathbf{M}_R and \mathbf{M}_I are associated, respectively, to dissipation and driving [69].)

We now rely on the third-quantization formalism [69, 70] to vectorize the Lindblad equation as

$$\frac{d}{dt}|\hat{\rho}\rangle = \hat{\mathcal{L}}|\hat{\rho}\rangle. \quad (\text{B10})$$

According to this formalism, one expands $|\hat{\rho}\rangle$ into a basis of vectors (Hermitian operators) $\{|P_\alpha\rangle\}$ of a $2^{2L} = 4^L$ -dimensional space:

$$|P_\alpha\rangle \stackrel{\text{def}}{=} 2^{-L/2} \check{c}_1^{\alpha_1} \dots \check{c}_{2L}^{\alpha_{2L}}, \quad \alpha_j = 0, 1. \quad (\text{B11})$$

We then define [69, 70] the action of fermionic superoperators on this space as follows:

$$\begin{cases} \hat{a}_j |P_\alpha\rangle = \delta_{\alpha_j,1} |\check{c}_j P_\alpha\rangle \\ \hat{a}_j^\dagger |P_\alpha\rangle = \delta_{\alpha_j,0} |\check{c}_j P_\alpha\rangle. \end{cases} \quad (\text{B12})$$

In terms of these, the Lindbladian can be represented as a quadratic superoperator of the form

$$\hat{\mathcal{L}} = (\hat{\mathbf{a}}^\dagger, \hat{\mathbf{a}}^\text{T}) \begin{pmatrix} -\mathbf{X}^\text{T} & i\mathbf{Y} \\ \mathbf{0} & \mathbf{X} \end{pmatrix} \begin{pmatrix} \hat{\mathbf{a}} \\ \hat{\mathbf{a}}^{\dagger\text{T}} \end{pmatrix} - \text{Tr}\mathbf{X} \quad (\text{B13})$$

Here, $\hat{\mathbf{a}} = (\hat{a}_1, \dots, \hat{a}_{2L})^\text{T}$ is a $2L$ -dimensional column vector formed with the \hat{a}_j operators, $\hat{\mathbf{a}}^\dagger = (\hat{a}_1^\dagger, \dots, \hat{a}_{2L}^\dagger)$ the corresponding row vector, the $2L \times 2L$ real matrix \mathbf{X} is given by

$$\mathbf{X} = -2i\mathbf{H}^M + 2\mathbf{M}_\text{R}. \quad (\text{B14})$$

and the $2L \times 2L$ real anti-symmetric matrix $\mathbf{Y} = 4\mathbf{M}_\text{I}$. Quite importantly, $\mathbf{X} + \mathbf{X}^\text{T} = 4\mathbf{M}_\text{R}$ is (semi)-positive definite.

Due to the upper triangular nature of the Lindbladian, its spectral properties are completely determined by the spectrum of \mathbf{X} , i.e., by the set of *rapidities* $\{\beta_j\}$ [69, 70], with $\text{Re}\beta_j \geq 0$. Hence, it is possible to state symmetry relations for \mathbf{X} that generalize the tenfold way classification of topological insulators [71, 72] when in interaction with an environment, as long as the dissipative dynamics can be described by quadratic Lindbladians. Like the Hamiltonian for closed systems, \mathbf{X} becomes now the landmark to check whether the symmetries are preserved or broken and, consequently, if the topological features of the open systems can be preserved or not. Indeed, for closed systems, according to the presence or absence of the following three time-reversal, particle-hole and chiral symmetries (TRS, PHS, Chiral)

$$\begin{aligned} \mathbf{H}^M &= \mathbf{U}_T \mathbf{H}^{M*} \mathbf{U}_T^\dagger & \mathbf{U}_T \mathbf{U}_T^* &= \pm \mathbf{1} & (\text{TRS}) \\ \mathbf{H}^M &= -\mathbf{U}_C \mathbf{H}^{M*} \mathbf{U}_C^\dagger & \mathbf{U}_C \mathbf{U}_C^* &= \pm \mathbf{1} & (\text{PHS}) \\ \mathbf{H}^M &= -\mathbf{U}_S \mathbf{H}^M \mathbf{U}_S^\dagger & \mathbf{U}_S^2 &= \mathbf{1} & (\text{Chiral}) \end{aligned} \quad (\text{B15})$$

where $\mathbf{U}_{T,C,S}$ are all unitary operators, and $\mathbf{U}_S = \mathbf{U}_C \mathbf{U}_T$, the systems fall in one of the ten symmetry classes related to specific types (\mathbb{Z} , \mathbb{Z}_2 , $2\mathbb{Z}$) of topological states, according to the dimension of the system [71]. For open systems, the generalized equations become

$$\begin{aligned} \mathbf{X} &= \mathbf{U}_T \mathbf{X}^T \mathbf{U}_T^\dagger & \mathbf{U}_T \mathbf{U}_T^* &= \pm \mathbf{1} & (\text{TRS}) \\ \mathbf{X} &= \mathbf{U}_C \mathbf{X}^* \mathbf{U}_C^\dagger & \mathbf{U}_C \mathbf{U}_C^* &= \pm \mathbf{1} & (\text{PHS}) \\ \mathbf{X} &= \mathbf{U}_S \mathbf{X}^\dagger \mathbf{U}_S^\dagger & \mathbf{U}_S^2 &= \mathbf{1} & (\text{PAH}) \end{aligned} \quad (\text{B16})$$

where the unitaries have to be the same as those of the closed classification and the Pseudo-Anti-Hermiticity (PAH) symmetry replaces Chiral symmetry. These equations are obtained imposing some physical constraints on the spectrum of the Lindbladian. According to this classification, it is possible to see that the jump operators in Eqs. (7) are symmetry-preserving, while the ones in Eq. (8) are symmetry-breaking.

3. Hamiltonian

Let us start considering the SSH Hamiltonian of Eq. (6). In Nambu formalism it reads as:

$$\hat{H}_{\text{SSH}} = \hat{\mathbf{C}}^\dagger \mathbf{H}_{\text{SSH}} \hat{\mathbf{C}} \quad , \quad (\text{B17})$$

with

$$\mathbf{H}_{\text{SSH}} = \begin{pmatrix} \mathbf{A}_H & \mathbf{0} \\ \mathbf{0} & -\mathbf{A}_H \end{pmatrix} \quad , \quad (\text{B18})$$

where the $L \times L$ real symmetric matrix \mathbf{A}_H reads:

$$\mathbf{A}_H = \frac{1}{2} \begin{pmatrix} 0 & -J_o & 0 & \cdots & \cdots & \cdots & 0 \\ -J_o & 0 & -J_e & 0 & \cdots & \cdots & 0 \\ 0 & -J_e & 0 & -J_o & 0 & \cdots & 0 \\ 0 & 0 & -J_o & 0 & -J_e & \cdots & 0 \\ \vdots & \vdots & \cdots & \ddots & \ddots & \ddots & 0 \\ \vdots & \vdots & \vdots & 0 & -J_e & 0 & -J_o \\ 0 & \cdots & \cdots & \cdots & 0 & -J_o & 0 \end{pmatrix} \quad . \quad (\text{B19})$$

Equivalently, in terms of Majorana operators:

$$\hat{H}_{\text{SSH}} = \hat{\mathbf{C}}^\dagger \mathbf{H}_{\text{SSH}} \hat{\mathbf{C}} = \tilde{\mathbf{c}}^T \mathbf{H}_{\text{SSH}}^M \tilde{\mathbf{c}} \quad . \quad (\text{B20})$$

with

$$\mathbf{H}_{\text{SSH}}^M = \frac{i}{2} \begin{pmatrix} \mathbf{0} & \mathbf{A}_H \\ -\mathbf{A}_H & \mathbf{0} \end{pmatrix} \quad . \quad (\text{B21})$$

The symmetries that hold for the SSH chain, written in terms of Majorana, are

$$\begin{aligned} \mathbf{H}_{\text{SSH}}^M &= -\mathbf{H}_{\text{SSH}}^{M*} = \mathbf{U}_T \mathbf{H}_{\text{SSH}}^M \mathbf{U}_T^\dagger & (\text{TRS}) \\ \mathbf{H}_{\text{SSH}}^M &= \Sigma_z \mathbf{H}_{\text{SSH}}^{M*} \Sigma_z = \\ &= -\mathbf{U}_T \Sigma_z \mathbf{H}_{\text{SSH}}^M (\mathbf{U}_T \Sigma_z)^\dagger & (\text{PHS}) \\ \mathbf{H}_{\text{SSH}}^M &= -\Sigma_z \mathbf{H}_{\text{SSH}}^M \Sigma_z^\dagger & (\text{Chiral}) \end{aligned} \quad (\text{B22})$$

where $\mathbf{U}_T = \Sigma_z$ and

$$\Sigma_z = \hat{\sigma}^z \otimes \mathbf{1} \quad (\text{B23})$$

so that $\mathbf{U}_C = \mathbf{U}_T \Sigma_z = \mathbf{1}$ is the operator related to the particle-hole symmetry (PHS) and $\mathbf{U}_S = \Sigma_z$ is the one related to the chiral symmetry (CS). These operators are properly the same we will use to check the symmetries in the dissipative case. The fact that the three symmetries are satisfied, together with the fact that

$$\begin{aligned} \mathbf{U}_T^2 &= \mathbf{U}_T \mathbf{U}_T^* = \mathbf{1} \\ \mathbf{U}_C^2 &= \mathbf{U}_C \mathbf{U}_C^* = \mathbf{1} \\ \mathbf{U}_S^2 &= \mathbf{1} \end{aligned} \quad (\text{B24})$$

makes the system fall into the topological class BDI which provides for a \mathbb{Z} -type of topological invariants, according to the periodic table of topological insulators [72].

4. SPD dynamics

In the SPD dynamics, the dissipation matrix, in terms of Majorana operators, is:

$$\mathbf{M} = \frac{\gamma}{4} \begin{pmatrix} \mathbf{1} & -i(\mathbf{1}_o - \mathbf{1}_e) \\ i(\mathbf{1}_o - \mathbf{1}_e) & \mathbf{1} \end{pmatrix} \quad . \quad (\text{B25})$$

where $\mathbf{1}_o$ is an identity only on the odd (A) sites, and similarly $\mathbf{1}_e$ for the even (B) sites, hence $\mathbf{1} = \mathbf{1}_o + \mathbf{1}_e$.

The real matrix \mathbf{X} appearing in Eq. (B14) is therefore given by:

$$\mathbf{X} \equiv -2i\mathbf{H}_{\text{SSH}}^{\text{M}} + 2\mathbf{M}_{\text{R}} = \begin{pmatrix} \frac{\gamma}{2}\mathbf{1} & \mathbf{A}_{\text{H}} \\ -\mathbf{A}_{\text{H}} & \frac{\gamma}{2}\mathbf{1} \end{pmatrix}. \quad (\text{B26})$$

The latter satisfies equations (B16) with the same unitaries of equations (B22).

5. SBD dynamics

In the SBD dynamics the dissipation matrix is:

$$\mathbf{M} = \frac{\gamma}{4} \begin{pmatrix} \mathbf{M}_{\text{A}} & -i\mathbf{M}_{\text{A}} \\ i\mathbf{M}_{\text{A}} & \mathbf{M}_{\text{A}} \end{pmatrix}, \quad (\text{B27})$$

with the complex $L \times L$ matrix \mathbf{M}_{A} given by:

$$\mathbf{M}_{\text{A}} = \begin{pmatrix} 1 & 1 & 0 & \dots & \dots & \dots & 0 \\ 1 & 2 & 1 & 0 & \dots & \dots & 0 \\ 0 & 1 & 2 & 1 & 0 & \dots & 0 \\ 0 & 0 & 1 & 2 & 1 & \dots & 0 \\ \vdots & \vdots & \dots & \ddots & \ddots & \ddots & 0 \\ \vdots & \vdots & \vdots & 0 & 1 & 2 & 1 \\ 0 & \dots & \dots & \dots & 0 & 1 & 1 \end{pmatrix}. \quad (\text{B28})$$

which does not allow to see the symmetries preserved for \mathbf{X} .

Appendix C: Free-fermions techniques

1. Quadratic Hamiltonians

Let us consider the most general form for a quadratic Hamiltonian

$$\hat{\Theta} = \sum_{i,j} \left[A_{i,j} \hat{c}_i^\dagger \hat{c}_j - A_{i,j}^* \hat{c}_i \hat{c}_j^\dagger + B_{i,j} \hat{c}_i \hat{c}_j - B_{i,j}^* \hat{c}_i^\dagger \hat{c}_j^\dagger \right], \quad (\text{C1})$$

where \mathbf{A} is a Hermitian matrix and \mathbf{B} is a skew-symmetric matrix. This general quadratic Hamiltonian can be also rewritten as [67]

$$\hat{\Theta} = \hat{\mathbf{C}}^\dagger \Theta \hat{\mathbf{C}}, \quad (\text{C2})$$

where

$$\Theta = \begin{pmatrix} \mathbf{A} & \mathbf{B} \\ -\mathbf{B}^* & \mathbf{A}^* \end{pmatrix} \quad (\text{C3})$$

and $\hat{\mathbf{C}}$ is the Nambu operator defined in Eq. (B1).

2. Gaussian states

A Gaussian state is any state whose density matrix can be written as

$$\hat{\rho}(t) = \frac{1}{\mathcal{Z}(t)} e^{-\hat{\Theta}(t)} \quad (\text{C4})$$

where $\mathcal{Z}(t) = \text{Tr} e^{-\hat{\Theta}(t)}$ enforces the normalization. For Gibbs states, $\hat{\Theta}$ is the real quadratic Hamiltonian of the equilibrium state, while, in general, it plays the role of an effective Hamiltonian, which we will refer to as *entanglement Hamiltonian*.

A simpler expression for the Gaussian state can be derived considering a number-preserving $\hat{\Theta}$, i.e.,

$$\hat{H}_{\text{np}} = \sum_{i,j} H_{i,j} \hat{c}_i^\dagger \hat{c}_j. \quad (\text{C5})$$

If $U_{k,\alpha}$ is the α -th component of the k -th eigenstate of \mathbf{H} with eigenvalues ϵ_k , the unitary transformation

$$\hat{c}_i = \sum_k U_{k,i} \hat{a}_k, \quad (\text{C6})$$

allows to diagonalise \hat{H}_{np} and write the Gaussian state as [65, 73]

$$\begin{aligned} \hat{\rho} &= \frac{1}{\mathcal{Z}} e^{-\sum_k \frac{\epsilon_k}{2} (\hat{a}_k^\dagger \hat{a}_k - \hat{a}_k \hat{a}_k^\dagger)} = \\ &= \bigotimes_{k=1}^N \frac{e^{-\frac{\epsilon_k}{2} (\hat{a}_k^\dagger \hat{a}_k - \hat{a}_k \hat{a}_k^\dagger)}}{\mathcal{Z}_k} = \bigotimes_{k=1}^N \frac{\hat{\rho}_k}{\mathcal{Z}_k}, \end{aligned} \quad (\text{C7})$$

where

$$\begin{aligned} \mathcal{Z}_k &= \text{Tr} \left[e^{\frac{\epsilon_k}{2} (\hat{a}_k^\dagger \hat{a}_k - \hat{a}_k \hat{a}_k^\dagger)} \right] = \\ &= 2 \cosh \epsilon_k / 2 = e^{\frac{\epsilon_k}{2}} + e^{-\frac{\epsilon_k}{2}}. \end{aligned} \quad (\text{C8})$$

It is thus trivial to derive the connection between the spectrum of the entanglement Hamiltonian and that of the density matrix.

3. Covariance matrix

As previously done, let us restrict our study to the number-preserving quadratic Hamiltonian of Eq. (C5). Let us consider the covariance matrix of Eq. (11) whose average is computed over the Gaussian state with effective Hamiltonian (C5).

Since $\hat{\rho}$ is a Gaussian state, Wick's theorem holds, and all the higher correlation functions can be expressed in terms of the Hermitian matrix \mathbf{G} . This means that the two-point covariance matrix \mathbf{G} encodes all the necessary information of the Gaussian state [7, 74]. As a limiting case, $\hat{\rho}$ can also be a pure state related to a Slater

determinant, i.e., an eigenstate of an effective Hamiltonian. Diagonalizing $\hat{\Theta}$ with the unitary transformation of Eq. (C6) means having

$$\sum_{i,j} U_{k,i}^* H_{i,j} U_{k',j} = \epsilon_k \delta_{k,k'}. \quad (\text{C9})$$

From the latter equation, we can derive

$$H_{i,j} = \sum_k U_{k,i}^* U_{k,j} \epsilon_k. \quad (\text{C10})$$

Considering Eq. (C10) and the Gaussian state of Eq. (C4), together with the Wick's theorem, we can obtain

$$G_{i,j} = \sum_k U_{k,i}^* U_{k,j} \frac{1}{1 + e^{\epsilon_k}}. \quad (\text{C11})$$

Comparing Eq. (C10) and Eq. (C11), we can deduce that the eigenvalues $\{\epsilon_k\}$ of \mathbf{H} and those $\{\zeta_k\}$ of \mathbf{G} are related by

$$\zeta_k = \frac{1}{1 + e^{\epsilon_k}}, \quad (\text{C12})$$

i.e.,

$$\mathbf{H} = \ln \left[\frac{\mathbf{1} - \mathbf{G}}{\mathbf{G}} \right]. \quad (\text{C13})$$

Eventually, what we have to do is diagonalizing the Hamiltonian. From the unitary diagonalisation matrix \mathbf{U} , we can find the expression of the effective creation and annihilation operators, so that

$$G_{i,j} = \langle \hat{c}_j^\dagger \hat{c}_i \rangle = \sum_{k,k'} \langle \hat{a}_{k'}^\dagger U_{k',j} U_{i,k}^* \hat{a}_k \rangle, \quad (\text{C14})$$

which means that

$$G_{i,j} = \sum_{k=1}^N U_{i,k}^* U_{k,j}, \quad (\text{C15})$$

where N is the number of particles we consider in the system, which, in our half-filling case at zero temperature, coincides with the number of unit cells of the chain.

This approach is faster than direct diagonalisation and allows to compute efficiently, – i.e., by the $N \times N$ matrix \mathbf{G} – the reduced density matrix and its entanglement spectra and S^D .

The representation of the reduced density matrix can be thus written as

$$\begin{aligned} \rho &= \bigotimes_{k=1}^N \frac{1}{\mathcal{Z}_k} \begin{pmatrix} \rho_{k11} & \rho_{k10} \\ \rho_{k01} & \rho_{k00} \end{pmatrix} = \\ &= \bigotimes_{k=1}^N \begin{pmatrix} \frac{e^{-\frac{\epsilon_k}{2}}}{e^{\frac{\epsilon_k}{2}} + e^{-\frac{\epsilon_k}{2}}} & 0 \\ 0 & \frac{e^{\frac{\epsilon_k}{2}}}{e^{\frac{\epsilon_k}{2}} + e^{-\frac{\epsilon_k}{2}}} \end{pmatrix} = \\ &= \bigotimes_{k=1}^N \begin{pmatrix} \zeta_k & 0 \\ 0 & (1 - \zeta_k) \end{pmatrix}, \end{aligned} \quad (\text{C16})$$

which leaves us with the sought connection between the spectra $\{\lambda_k\}$ of ρ and $\{\zeta_k\}$ of \mathbf{G} .

4. Reduced system

When we consider a subsystem of $\{\alpha, \beta\} \in X$ sites, the reduced density matrix $\hat{\rho}_X$ allows to reproduce all expectation values in the subsystem and, as long as it remains Gaussian, so does the *reduced two-point covariance matrix*

$$G_{X\alpha,\beta} = \text{Tr}(\hat{\rho}_X \hat{c}_\beta^\dagger \hat{c}_\alpha). \quad (\text{C17})$$

In order for $\hat{\rho}_X$ to be Gaussian, it is still required to be the exponential of a quadratic effective Hamiltonian, i.e.,

$$\hat{\rho}_X = \mathcal{K} e^{-\hat{H}_X}, \quad (\text{C18})$$

with

$$\hat{H}_X = \sum_{\alpha,\beta} H_{X\alpha,\beta} \hat{c}_\alpha^\dagger \hat{c}_\beta. \quad (\text{C19})$$

Computing the spectrum of the reduced correlation matrix (C17) is equivalent to exactly diagonalizing the entanglement Hamiltonian of the reduced density matrix (C18), yet faster.

Appendix D: Treating the degeneracy of the edge modes

In the preparation of the initial state for the dynamics, we encounter a numerical issue due to the edge mode degeneracy. Specifically, when diagonalizing the Hamiltonian, we find two states with energies close to zero, separated by a gap that decreases exponentially with the system size. Due to this degeneracy, diagonalization routines arbitrarily combine the two eigenstates associated with the nearly degenerate eigenvalue. This leads to problems in constructing the initial correlator, as the zero-energy eigenstates are arbitrarily ordered and combined. As a consequence, the DEE in the initial state is not equal to 2. To overcome this issue, we decide to exploit the parity symmetry of the Hamiltonian.

Indeed, we know that $[\hat{H}_{\text{SSH}}, \hat{P}] = 0$ where \hat{P} is the parity operator whose matrix representation in one dimension acts as

$$\mathbf{P} = \begin{pmatrix} 0 & 0 & \cdots & 0 & 1 \\ 0 & 0 & \cdots & 1 & 0 \\ & & \ddots & & \\ 0 & 1 & \cdots & 0 & 0 \\ 1 & 0 & \cdots & 0 & 0 \end{pmatrix}, \quad (\text{D1})$$

so to invert the first with the last site, the second with the second-last site and so on. Due to this symmetry relation of the SSH Hamiltonian, since both \hat{H}_{SSH} and \hat{P}

are Hermitian, we know it is possible to find a common basis of eigenvectors \mathbf{V}_P such that \mathbf{P} becomes diagonal and \mathbf{H}_{SSH} is reduced into two diagonal blocks of different parity, i.e., $\mathbf{H}_P = \mathbf{V}_P^T \mathbf{H}_{\text{SSH}} \mathbf{V}_P$ such that

$$\mathbf{H}_P = \begin{pmatrix} \mathbf{H}_{\text{odd}} & \\ & \mathbf{H}_{\text{even}} \end{pmatrix}. \quad (\text{D2})$$

Reducing the Hamiltonian into two blocks allows us to split the two degenerate zero modes — one will go in the even block and the other in odd block. Hence, we can diagonalize the two blocks and find the eigenvectors, \mathbf{U}_{odd} and \mathbf{U}_{even} , separately, so to avoid arbitrary numerical superpositions of the two quasi-zero-energy modes. The total matrix of eigenvectors in the rotated basis is

$$\mathbf{U}_P = \begin{pmatrix} \mathbf{U}_{\text{odd}} & \\ & \mathbf{U}_{\text{even}} \end{pmatrix}. \quad (\text{D3})$$

When ordering the eigenvalues in ascending order, we treat the two near-zero-energy modes as degenerate since they differ only beyond the threshold of machine precision ($\sim 10^{-12}$). We place the zero mode of the even block first, followed by the odd-block one. This is because, when constructing the ground state correlator at half-filling, we will sum over all negative energy modes from both the even and odd blocks, up to the sole even zero mode. We choose to populate only the even mode to achieve a spatial configuration of the Bell-like pair between the two edge modes that corresponds to a triplet state $\frac{1}{\sqrt{2}}(|0_1, 1_L\rangle + |1_1, 0_L\rangle)$. Once the eigenvalues and

eigenstates are ordered in the rotated basis, we return to the original basis by rotating the eigenstates with \mathbf{V}_P . With these eigenstates, we can finally construct the ground state correlator at half-filling.

Appendix E: Details on the quantum-jump unraveling for quadratic Lindblad equations

1. Quantum-jump unraveling for Gaussian states

We refer to Ref. [75] for more information regarding the adopted algorithm for the computation of the quantum-jump trajectory. Suitably arranging the latter, exploiting the Gaussian nature of the states we deal with, we actually apply the algorithm directly on the covariance matrix related to the Gaussian state, which results in an enormous advantage in terms of computational cost of our calculations. Specifically, we look at the time evolution of $\mathbf{G}(t)|_{\text{traj}}$. In the following we will name $\mathbf{G}(t)|_{\text{traj}}$ as $\mathbf{G}(t)$, for brevity. Nevertheless, it is important to stress that, in the main text, $\mathbf{G}(t)$ is the average over many realizations of $\mathbf{G}(t)|_{\text{traj}}$.

a. Non-Hermitian evolution

Let us now consider the non-Hermitian contribution to the evolution ruled by \hat{H}_{eff} . An efficient way of updating the state when the non-Hermitian evolution occurs is considering

$$\mathbf{G}(t + dt) = \langle \psi(t) | \left(\hat{\mathbf{1}} + i\hat{H}_{\text{eff}}^\dagger dt + \Lambda(t)\delta t \right) \hat{c}_j^\dagger \hat{c}_i \left(\hat{\mathbf{1}} - i\hat{H}_{\text{eff}} dt + \Lambda(t)dt \right) | \psi(t) \rangle + o(dt) \quad (\text{E1})$$

is the part of equation (1) ruling the non-Hermitian evolution of the correlation function including the normalization of the state, valid in $o(dt)$ limit, where we have written

$$\hat{\Lambda} = \frac{\gamma}{2} \sum_k \hat{L}_k^\dagger \hat{L}_k \quad (\text{E2a})$$

$$\Lambda = \langle \psi(t) | \hat{\Lambda} | \psi(t) \rangle \quad (\text{E2b})$$

$$\hat{H}_{\text{eff}} = \hat{H}_{\text{SSH}} - i\hat{\Lambda}. \quad (\text{E2c})$$

This leads to

$$G_{ij}(t + dt) = G_{ij}(t) + idt \langle \psi(t) | [\hat{H}_{\text{SSH}}, \hat{c}_j^\dagger \hat{c}_i] | \psi(t) \rangle - dt \langle \psi(t) | \left\{ \hat{\Lambda}, \hat{c}_j^\dagger \hat{c}_i \right\} | \psi(t) \rangle + 2dt \Lambda G_{ij}(t) + o(dt). \quad (\text{E3})$$

What makes symmetry-breaking and symmetry-preserving case different is $\hat{\Lambda}$, so we will write them in the following. For the unitary part, which is common to

both dynamics, we have

$$\langle [\hat{H}_{\text{SSH}}, \hat{c}_j^\dagger \hat{c}_i] \rangle = \sum_\alpha (G_{i,\alpha} H_{\alpha,j} - H_{i,\alpha} G_{\alpha,j}) \quad (\text{E4})$$

2. Evolution of the norm

In order to consider the occurrence of the quantum jump when $\langle \psi(t^*) | \psi(t^*) \rangle > r$, where r is the random number uniformly distributed in $[0, 1]$, we simultaneously compute the time-evolution of the norm $n(t) = \langle \psi(t) | \psi(t) \rangle$ when it evolves under \hat{H}_{eff}

$$n(t + dt) = n(dt) - 2dt n(t) \Lambda(t) + o(dt), \quad (\text{E5})$$

so that

$$\frac{n(t + dt) - n(t)}{dt} = -2\Lambda(t)n(t), \quad (\text{E6})$$

which in $dt \rightarrow 0$ limit is

$$\frac{dn(t)}{dt} = -2\Lambda(t)n(t), \quad (\text{E7})$$

where, again, Λ must be computed in the two dissipative cases.

a. SPD

a.1. Non-Hermitian evolution. In the SPD case we have

$$\hat{\Lambda} = \frac{\gamma}{2} \left[\sum_{\alpha=1}^L (-1)^\alpha \hat{c}_\alpha^\dagger \hat{c}_\alpha \right] + L \frac{\gamma}{4} \quad (\text{E8})$$

$$G_{ij}(t + dt) = \langle \psi_{t+dt} | \hat{c}_j^\dagger \hat{c}_i | \psi_{t+dt} \rangle = \frac{\langle \psi_t | \hat{c}_{2l-1}^\dagger \hat{c}_j^\dagger \hat{c}_i \hat{c}_{2l-1} | \psi_t \rangle}{G_{2l-1, 2l-1}(t)} = G_{ij}(t) + \frac{F_{2l-1, j}^*(t) F_{2l-1, i}(t) - G_{i, 2l-1}(t) G_{2l-1, j}(t)}{G_{2l-1, 2l-1}(t)} \quad (\text{E12})$$

$$F_{ij}(t + dt) = \langle \psi_{t+dt} | \hat{c}_j \hat{c}_i | \psi_{t+dt} \rangle = \frac{\langle \psi_t | \hat{c}_{2l-1}^\dagger \hat{c}_j \hat{c}_i \hat{c}_{2l-1} | \psi_t \rangle}{G_{2l-1, 2l-1}(t)} = F_{ij}(t) + \frac{G_{j, 2l-1}(t) F_{2l-1, i}(t) - G_{i, 2l-1}(t) F_{2l-1, j}(t)}{G_{2l-1, 2l-1}(t)}. \quad (\text{E13})$$

- For one $l = 1, \dots, N$, with probability

$$dq_l = \gamma dt \langle \psi_t | \hat{c}_{lB} \hat{c}_{lB}^\dagger | \psi_t \rangle = \gamma dt [1 - G_{2l, 2l}(t)],$$

we apply the transformation

$$|\psi_t\rangle \longrightarrow |\psi_{t+dt}\rangle = \frac{\hat{c}_{2l}^\dagger |\psi_t\rangle}{\|\hat{c}_{2l}^\dagger |\psi_t\rangle\|}.$$

$$G_{ij}(t + dt) = \langle \psi_{t+dt} | \hat{c}_j^\dagger \hat{c}_i | \psi_{t+dt} \rangle = \frac{\langle \psi_t | \hat{c}_{2l} \hat{c}_j^\dagger \hat{c}_i \hat{c}_{2l}^\dagger | \psi_t \rangle}{1 - G_{2l, 2l}(t)} = G_{ij}(t) + \frac{[\delta_{2lj} - G_{2lj}(t)][\delta_{i2l} - G_{i2l}(t)] - F_{i2l}(t) F_{j2l}^*(t)}{1 - G_{2l, 2l}(t)} \quad (\text{E14})$$

which leads to a non-Hermitian evolution of \mathbf{G} of the form

$$\frac{d\mathbf{G}}{dt} = i(\mathbf{G}\mathbf{H} - \mathbf{H}\mathbf{G}) - \gamma \left[\frac{\mathbf{G}\mathbf{S} + \mathbf{S}\mathbf{G}}{2} - \mathbf{G}\mathbf{S}\mathbf{G} \right], \quad (\text{E9})$$

where $\mathbf{S} = \mathbf{1}_o - \mathbf{1}_e$.

a.2. Quantum Jump. In the symmetry-preserving case we have jump operators of the form (7). We discretize the time at intervals dt . At each time step, we call $|\psi_t\rangle$ the state before the time step is performed, define $\hat{c}_{2j-1} = \hat{c}_{j,A}$, $\hat{c}_{2j} = \hat{c}_{j,B}$ and the time-dependent covariance matrix and anomalous covariance matrix, respectively as

$$G_{i,j}(t) \equiv \langle \psi_t | \hat{c}_j^\dagger \hat{c}_i | \psi_t \rangle, \quad F_{i,j}(t) \equiv \langle \psi_t | \hat{c}_j \hat{c}_i | \psi_t \rangle. \quad (\text{E10})$$

In order to perform the time step, we act on $|\psi_t\rangle$. There are some mutually exclusive possibilities

- For one $l = 1, \dots, N$, with probability

$$dp_l = \gamma dt \langle \psi_t | \hat{c}_{lA}^\dagger \hat{c}_{lA} | \psi_t \rangle = \gamma dt G_{2l-1, 2l-1}(t),$$

we apply the transformation

$$|\psi_t\rangle \longrightarrow |\psi_{t+dt}\rangle = \frac{\hat{c}_{2l-1} |\psi_t\rangle}{\|\hat{c}_{2l-1} |\psi_t\rangle\|}. \quad (\text{E11})$$

Assuming that the state remains Gaussian and that the Wick's theorem holds, this equation translates into an evolution equation for the covariance matrix

This reflects into a transformation for the correlation functions

$$F_{ij}(t + \Delta t) = \langle \psi_{t+\Delta t} | \hat{c}_j \hat{c}_i | \psi_{t+\Delta t} \rangle = \frac{\langle \psi_t | \hat{c}_{2l} \hat{c}_j \hat{c}_i \hat{c}_{2l}^\dagger | \psi_t \rangle}{1 - G_{2l, 2l}(t)} = F_{ij}(t) + \frac{F_{j 2l}(t)[\delta_{j 2l} - G_{i 2l}] - F_{i 2l}[\delta_{j 2l} - G_{j 2l}(t)]}{1 - G_{2l, 2l}(t)}. \quad (\text{E15})$$

b. SBD

b.1. Non-Hermitian evolution. In the symmetry-breaking case we have

$$\hat{\Lambda} = \frac{\gamma}{2} \left[\sum_{\alpha=0}^{L-2} \hat{c}_\alpha^\dagger \hat{c}_\alpha + \hat{c}_{\alpha+1}^\dagger \hat{c}_{\alpha+1} + \hat{c}_{\alpha+1}^\dagger \hat{c}_\alpha + \hat{c}_\alpha^\dagger \hat{c}_{\alpha+1} \right]. \quad (\text{E16})$$

From which it is straightforward to derive the non-Hermitian evolution of \mathbf{G} as done in the SPD dynamics.

b.2. Quantum Jump. In the symmetry-breaking case we have the jump operators of the form (8). In this case, we can write $\hat{c}_{2j-1} = \hat{c}_{jA}$, $\hat{c}_{2j} = \hat{c}_{jB}$. The mutually exclusive possibilities are

- For one $l = 1, \dots, N$ with probability

$$dp_l = \gamma dt \langle \psi_t | \hat{L}_{2l-1}^\dagger \hat{L}_{2l-1} | \psi_t \rangle = \gamma dt [G_{2l-1, 2l-1} + G_{2l, 2l} + G_{2l, 2l-1} + G_{2l-1, 2l}] = \gamma dt N \quad (\text{E17})$$

we apply the transformation

$$|\psi_t\rangle \rightarrow |\psi_{t+dt}\rangle = \frac{\hat{L}_{2l-1} |\psi_t\rangle}{\|\hat{L}_{2l-1} |\psi_t\rangle\|} = \frac{(\hat{c}_{2l-1} + \hat{c}_{2l}) |\psi_t\rangle}{\|\hat{c}_{2l-1} + \hat{c}_{2l} |\psi_t\rangle\|}$$

So that the correlation matrix, neglecting the anomalous correlations, becomes

$$G_{i,j}(t + dt) = G_{ij} - \frac{1}{N} \{G_{i, 2l-1} G_{2l-1, j} + G_{i, 2l} G_{2l, j} + G_{i, 2l} G_{2l-1, j} + G_{i, 2l-1} G_{2l, j}\} \quad (\text{E18})$$

- For one $l = 1, \dots, N$ with probability

$$dq_l = \gamma dt [G_{2l, 2l} + G_{2l+1, 2l+1} + G_{2l+1, 2l} + G_{2l, 2l+1}] = \gamma dt N \quad (\text{E19})$$

we apply the transformation

$$|\psi_t\rangle \rightarrow |\psi_{t+dt}\rangle = \frac{\hat{L}_{2l} |\psi_t\rangle}{\|\hat{L}_{2l} |\psi_t\rangle\|} = \frac{(\hat{c}_{2l} + \hat{c}_{2l+1}) |\psi_t\rangle}{\|\hat{c}_{2l} + \hat{c}_{2l+1} |\psi_t\rangle\|}$$

So that the correlation matrix, still neglecting the anomalous correlations, becomes

$$G_{i,j}(t + dt) = G_{ij} - \frac{1}{N} \{G_{i, 2l} G_{2l, j} + G_{i, 2l+1} G_{2l+1, j} + G_{i, 2l+1} G_{2l, j} + G_{i, 2l} G_{2l+1, j}\}. \quad (\text{E20})$$

Appendix F: Effect of the first jump on a 4-sites chain

In the following, we report the effect of the first jump on the ground state of the Hamiltonian in the perfectly-

dimerized topological state for a simple example of 4-

sites chain. Although extremely simplistic, this example helps understanding the origin of some of the peaks highlighted in the histograms of the index-resolved statistical analysis, in particular the peak at $\Delta S^D = -2$ for the global SPD dynamics and that at $\Delta S^D \simeq -0.38$ for the global SBD dynamics. The simplification of considering the jump as occurring as soon as the initial state is prepared is justified by the observation that the non-Hermitian evolution statistically does not drastically change the amount of entanglement of the initial state.

Let us consider a chain of two unit cells and four sites. We naturally choose a bipartition of the system such that the first two sites belong to \mathcal{A} and the last two belong to \mathcal{B} . Let us consider the local jump operator that acts on the first site of the chain so to give the non-normalized state

$$\begin{aligned} |\psi_{\text{jump}}^{\text{SPD}}\rangle &= \hat{c}_1 |\text{GS}\rangle = \hat{c}_1 \frac{1}{2} (\hat{c}_1^\dagger + \hat{c}_4^\dagger) (\hat{c}_2^\dagger + \hat{c}_3^\dagger) |0\rangle = \\ &= \frac{1}{2} (\hat{c}_2^\dagger + \hat{c}_3^\dagger) |0\rangle, \end{aligned} \quad (\text{F1})$$

which we will write in the following as

$$|\psi_{\text{jump}}^{\text{SPD}}\rangle = \frac{1}{2} (|1_2\rangle + |1_3\rangle). \quad (\text{F2})$$

In this notation, each state has implicit zero-occupation values on the non-written sites, e.g., $|1_2\rangle$ is implicitly equivalent to $|0_1 1_2 0_3 0_4\rangle$. The corresponding and suitably normalized density matrix will be

$$\begin{aligned} \hat{\rho}_{\text{jump}}^{\text{SPD}} &= |\psi_{\text{jump}}^{\text{SPD}}\rangle \langle \psi_{\text{jump}}^{\text{SPD}}| = \\ &= \frac{1}{2} (|1_2\rangle \langle 1_2| + |1_2\rangle \langle 1_3| + |1_3\rangle \langle 1_2| + |1_3\rangle \langle 1_3|). \end{aligned} \quad (\text{F3})$$

We can then compute the reduced density matrix, so to know the effect of the jump on one of the terms that make up the DEE. In doing the partial trace of this fermionic system we do not encounter ambiguities, since the states we deal with are always superposition of kets of a number of fermions of same (odd) parity [76, 77]. Hence, we trace out the degrees of freedom of sites 3 and 4 and obtain

$$\hat{\rho}_{\mathcal{A}}^{\text{SPD}} = \frac{1}{2} (|0_1 1_2\rangle \langle 0_1 1_2| + |0_1 0_2\rangle \langle 0_1 0_2|), \quad (\text{F4})$$

and its eigenvalues are $\{1/2, 1/2, 0, 0\}$ so that $S_{\mathcal{A}} = 1$ and $\Delta S_{\mathcal{A}} = -1$. Tracing out the degrees of freedom of sites 1,2 and 3 we can also compute the variation of $S_{\mathcal{A}\cup\mathcal{B}}$ since

$$\hat{\rho}_{\mathcal{A}\cup\mathcal{B}}^{\text{SPD}} = \frac{1}{2} (|0_3\rangle \langle 0_3| + |1_3\rangle \langle 1_3|) \quad (\text{F5})$$

so that $S_{\mathcal{A}\cup\mathcal{B}} = 1$ and $\Delta S_{\mathcal{A}\cup\mathcal{B}} = 0$. We can straightforwardly show that $\Delta S_{\mathcal{B}} = -1$ and $\Delta S_{\mathcal{A}\cap\mathcal{B}} = 0$ so to understand why the peak at $\Delta S^D = -2$ in Figs. 10(a) and 12(a) is due to the jump localized at one of the two edge sites.

On the other hand, if the SBD jump operator acts on the first site, without loss of generality, it simultaneously

affects the second site, so that the effect of the first jump on the boundary is completely different. In this case, after the jump, we have the non-normalized state

$$\begin{aligned} |\psi_{\text{jump}}^{\text{SBD}}\rangle &= \frac{1}{2} (\hat{c}_1 + \hat{c}_2) (\hat{c}_1^\dagger + \hat{c}_4^\dagger) (\hat{c}_2^\dagger + \hat{c}_3^\dagger) |0\rangle = \\ &= \frac{1}{2} [(\hat{c}_2^\dagger + \hat{c}_3^\dagger) - (\hat{c}_1^\dagger + \hat{c}_4^\dagger)] |0\rangle. \end{aligned} \quad (\text{F6})$$

In this case, there is still a trace of the long-range-entangled Bell-like state $\frac{1}{\sqrt{2}} (\hat{c}_1^\dagger + \hat{c}_4^\dagger)$, which causes a totally different and non-discrete variation in the entanglement contributions of the DEE. The corresponding normalized density matrix is

$$\begin{aligned} \hat{\rho}_{\text{jump}}^{\text{SBD}} &= \frac{1}{4} [|1_2\rangle \langle 1_2| + |1_2\rangle \langle 1_3| - |1_2\rangle \langle 1_1| + \\ &\quad - |1_2\rangle \langle 1_4| + |1_3\rangle \langle 1_2| + |1_3\rangle \langle 1_3| - |1_3\rangle \langle 1_1| + \\ &\quad - |1_3\rangle \langle 1_4| - |1_1\rangle \langle 1_2| - |1_1\rangle \langle 1_3| + |1_1\rangle \langle 1_1| + \\ &\quad + |1_1\rangle \langle 1_4| - |1_4\rangle \langle 1_2| - |1_4\rangle \langle 1_3| + |1_4\rangle \langle 1_1| + \\ &\quad + |1_4\rangle \langle 1_4|]. \end{aligned} \quad (\text{F7})$$

By tracing out the degrees of freedom of sites 3 and 4, we get

$$\begin{aligned} \hat{\rho}_{\mathcal{A}}^{\text{SBD}} &= \frac{1}{4} [2 |0_1 0_2\rangle \langle 0_1 0_2| + |0_1 1_2\rangle \langle 0_1 1_2| + \\ &\quad - |0_1 1_2\rangle \langle 1_1 0_2| - |1_1 0_2\rangle \langle 0_1 1_2| + |1_1 0_2\rangle \langle 1_1 0_2|], \end{aligned} \quad (\text{F8})$$

whose eigenvalues are $\{1/2, 1/2, 0, 0\}$ so that $S_{\mathcal{A}} = 1$ and $\Delta S_{\mathcal{A}} = -1$. This result is interesting since, after the occurrence of the jump on the boundary, one would expect $S_{\mathcal{A}}$ to go to 0 owing to the action on both the sites 1 and 2 that are part of two distinct Bell-like pairs. On the contrary, the peculiar form of $|\psi_{\text{jump}}^{\text{SBD}}\rangle$ mixes the things in an unexpectable way. Furthermore, we can trace out the degrees of freedom of sites 1, 2 and 3 and see that

$$\hat{\rho}_{\mathcal{A}\cup\mathcal{B}}^{\text{SBD}} = \frac{1}{4} [3 |0_3\rangle \langle 0_3| + |1_3\rangle \langle 1_3|] \quad (\text{F9})$$

so that $S_{\mathcal{A}\cup\mathcal{B}} = -\frac{3}{4} \log_2(3) + 2 \simeq 0.81$ and $\Delta S_{\mathcal{A}\cup\mathcal{B}} = -\frac{3}{4} \log_2(3) + 1 \simeq -0.19$. Again, counter-intuitively, the variation is not quantized, and we have numerically verified that, in the limit of perfectly-dimerized chain, this is not a size-dependent result. Again, it is straightforward to show that $\Delta S_{\mathcal{B}} \simeq -1$ and $\Delta S_{\mathcal{A}\cap\mathcal{B}} = -\frac{3}{4} \log_2(3) + 1 \simeq -0.19$ so that $\Delta S^D = 2(-\frac{3}{4} \log_2(3) + 2) \simeq 1.62$. This result is mainly useful to understand that the variation of the DEE in the SBD dynamics is not discrete when the first jump occurs. At the same time, analyzing a single trajectory at larger sizes shows that the variation, although still not discrete, is different and such that $\Delta S^D = 2 - 2(-\frac{3}{4} \log_2(3) + 2) \simeq -0.38$ because $\Delta S_{\mathcal{A}} = -\frac{3}{4} \log_2(3) + 1 \simeq -0.19$, $\Delta S_{\mathcal{B}} = -\frac{3}{4} \log_2(3) + 1 \simeq -0.19$, $\Delta S_{\mathcal{A}\cup\mathcal{B}} \simeq 0$ and $\Delta S_{\mathcal{A}\cap\mathcal{B}} \simeq 0$. This considerations help us in the interpretation of the peak at $\Delta S^D = 2 - 2(-\frac{3}{4} \log_2(3) + 2) \simeq -0.38$ in Figs. 10(c)

and 12(b). At the same time, we have numerically verified that the peak at $\Delta S^D = -2$ for the SBD dynamics is due to jumps occurring at the boundary after several

other jumps, and thus are not directly involved in the initial destruction of the long-range entangled Bell-like state.

-
- [1] B. Bernevig and T. Hughes, *Topological Insulators and Topological Superconductors* (Princeton University Press, 2013).
- [2] Y. Ashida, Z. Gong, and M. Ueda, *Advances in Physics* **69**, 249–435 (2020).
- [3] N. Okuma and M. Sato, *Annual Review of Condensed Matter Physics* **14**, 83–107 (2023).
- [4] S. Diehl, E. Rico, M. A. Baranov, and P. Zoller, *Nature Physics* **7**, 971–977 (2011).
- [5] C.-E. Bardyn, M. A. Baranov, C. V. Kraus, E. Rico, A. İmamoglu, P. Zoller, and S. Diehl, *New Journal of Physics* **15**, 085001 (2013).
- [6] S. Lieu, M. McGinley, and N. R. Cooper, *Phys. Rev. Lett.* **124**, 040401 (2020).
- [7] A. Altland, M. Fleischhauer, and S. Diehl, *Phys. Rev. X* **11**, 021037 (2021).
- [8] A. Altland and M. R. Zirnbauer, *Physical Review B* **55**, 1142 (1997).
- [9] K. Kawabata, K. Shiozaki, M. Ueda, and M. Sato, *Phys. Rev. X* **9**, 041015 (2019).
- [10] D. Bernard and A. LeClair, A classification of non-hermitian random matrices, in *Statistical Field Theories* (Springer Netherlands, 2002) p. 207–214.
- [11] T. Prosen, *Phys. Rev. Lett.* **109**, 090404 (2012).
- [12] B. Buca and T. Prosen, *New Journal of Physics* **14**, 073007 (2012).
- [13] V. V. Albert and L. Jiang, *Phys. Rev. A* **89**, 022118 (2014).
- [14] J. Huber, P. Kirton, S. Rotter, and P. Rabl, *SciPost Phys.* **9**, 052 (2020).
- [15] M. Kawasaki, K. Mochizuki, and H. Obuse, *Phys. Rev. B* **106**, 035408 (2022).
- [16] L. Mao, F. Yang, and H. Zhai, *Reports on Progress in Physics* **87**, 070501 (2024).
- [17] F. K. Kunst, E. Edvardsson, J. C. Budich, and E. J. Bergholtz, *Phys. Rev. Lett.* **121**, 026808 (2018).
- [18] Z. Gong, Y. Ashida, K. Kawabata, K. Takasan, S. Higashikawa, and M. Ueda, *Phys. Rev. X* **8**, 031079 (2018).
- [19] H. Shen, B. Zhen, and L. Fu, *Phys. Rev. Lett.* **120**, 146402 (2018).
- [20] O. Viyuela, A. Rivas, and M. A. Martin-Delgado, *Phys. Rev. Lett.* **112**, 130401 (2014).
- [21] O. Viyuela, A. Rivas, S. Gasparinetti, A. Wallraff, S. Filipp, and M. A. Martin-Delgado, *npj Quantum Information* **4**, 10 (2018).
- [22] A. Carollo, B. Spagnolo, and D. Valenti, (2017), [arXiv:1710.07560](https://arxiv.org/abs/1710.07560).
- [23] C.-E. Bardyn, L. Wawer, A. Altland, M. Fleischhauer, and S. Diehl, *Phys. Rev. X* **8**, 011035 (2018).
- [24] R. Unanyan, M. Kiefer-Emmanouilidis, and M. Fleischhauer, *Phys. Rev. Lett.* **125**, 215701 (2020).
- [25] Z.-M. Huang and S. Diehl, (2024), [arXiv:2401.10993](https://arxiv.org/abs/2401.10993).
- [26] D. Chen, S. Chesi, and M.-S. Choi, *Universal entanglement revival of topological origin* (2024), [arXiv:2410.17562](https://arxiv.org/abs/2410.17562).
- [27] A. Nava, G. Campagnano, P. Sodano, and D. Giuliano, *Phys. Rev. B* **107**, 035113 (2023).
- [28] E. G. Cinnirella, A. Nava, G. Campagnano, and D. Giuliano, *Phys. Rev. B* **109**, 035114 (2024).
- [29] H. Carmichael, *Statistical Methods in Quantum Optics 1: Master Equations and Fokker-Planck Equations*, Theoretical and Mathematical Physics (Springer Berlin Heidelberg, 2013).
- [30] A. J. Daley, *Advances in Physics* **63**, 77–149 (2014).
- [31] M. B. Plenio and P. L. Knight, *Reviews of Modern Physics* **70**, 101–144 (1998).
- [32] K. Mølmer, Y. Castin, and J. Dalibard, *J. Opt. Soc. Am. B* **10**, 524 (1993).
- [33] H. P. Breuer and F. Petruccione, *The theory of open quantum systems* (Oxford University Press, Great Clarendon Street, 2002).
- [34] Y. Li, X. Chen, and M. P. A. Fisher, *Phys. Rev. B* **98**, 205136 (2018).
- [35] B. Skinner, J. Ruhman, and A. Nahum, *Phys. Rev. X* **9**, 031009 (2019).
- [36] A. C. Potter and R. Vasseur, Entanglement dynamics in hybrid quantum circuits, in *Entanglement in Spin Chains: From Theory to Quantum Technology Applications*, edited by A. Bayat, S. Bose, and H. Johanneson (Springer International Publishing, Cham, 2022) pp. 211–249.
- [37] R. Fazio, J. Keeling, L. Mazza, and M. Schirò, *Many-body open quantum systems* (2024), [arXiv:2409.10300](https://arxiv.org/abs/2409.10300) [quant-ph].
- [38] B. Zeng, X. Chen, D. Zhou, and X. Wen, *Quantum Information Meets Quantum Matter: From Quantum Entanglement to Topological Phases of Many-Body Systems*, Quantum science and technology (Springer New York, 2019).
- [39] J. Chen, Z. Ji, C.-K. Li, Y.-T. Poon, Y. Shen, N. Yu, B. Zeng, and D. Zhou, *New Journal of Physics* **17**, 083019 (2015).
- [40] S. V. Isakov, M. B. Hastings, and R. G. Melko, *Nature Physics* **7**, 772–775 (2011).
- [41] H.-C. Jiang, Z. Wang, and L. Balents, *Nature Physics* **8**, 902–905 (2012).
- [42] A. Kitaev and J. Preskill, *Phys. Rev. Lett.* **96**, 110404 (2006).
- [43] M. Levin and X.-G. Wen, *Phys. Rev. Lett.* **96**, 110405 (2006).
- [44] G. Torre, J. Odavić, P. Fromholz, S. M. Giampaolo, and F. Franchini, *SciPost Phys. Core* **7**, 050 (2024).
- [45] A. Arora, A. Kejriwal, and B. Muralidharan, (2023), [arXiv:2303.03837](https://arxiv.org/abs/2303.03837).
- [46] H. Pichler, G. Zhu, A. Seif, P. Zoller, and M. Hafezi, *Phys. Rev. X* **6**, 041033 (2016).
- [47] A. Elben, B. Vermersch, M. Dalmonte, J. I. Cirac, and P. Zoller, *Phys. Rev. Lett.* **120**, 050406 (2018).
- [48] T. Brydges, A. Elben, P. Jurcevic, B. Vermersch, C. Maier, B. P. Lanyon, P. Zoller, R. Blatt, and C. F. Roos, *Science* **364**, 260 (2019).
- [49] P. Fromholz, G. Magnifico, V. Vitale, T. Mendes-Santos,

- and M. Dalmonte, *Phys. Rev. B* **101**, 085136 (2020).
- [50] T. Micallo, V. Vitale, M. Dalmonte, and P. Fromholz, *SciPost Phys. Core* **3**, 012 (2020).
- [51] S. Mondal, D. Sen, and A. Dutta, *Journal of Physics: Condensed Matter* **35**, 085601 (2022).
- [52] W. P. Su, J. R. Schrieffer, and A. J. Heeger, *Phys. Rev. Lett.* **42**, 1698 (1979).
- [53] W. P. Su, J. R. Schrieffer, and A. J. Heeger, *Phys. Rev. B* **22**, 2099 (1980).
- [54] M. Z. Hasan and C. L. Kane, *Reviews of Modern Physics* **82**, 3045–3067 (2010).
- [55] X.-L. Qi and S.-C. Zhang, *Reviews of Modern Physics* **83**, 1057–1110 (2011).
- [56] J. K. Asbóth, L. Oroszlány, and A. Pályi, *A Short Course on Topological Insulators* (Springer International Publishing, 2016).
- [57] Y. Le Gal, X. Turkeshi, and M. Schirò, *PRX Quantum* **5**, 030329 (2024).
- [58] G. Lindblad, *Communications in Mathematical Physics* **48**, 119 (1976).
- [59] D. S. Simon, S. Osawa, and A. V. Sergienko, *Journal of Physics: Condensed Matter* **31**, 045001 (2018).
- [60] M. V. Berry, *Proceedings of the Royal Society of London. A. Mathematical and Physical Sciences* **392**, 45 (1984).
- [61] J. Zak, *Phys. Rev. Lett.* **62**, 2747 (1989).
- [62] H. Schomerus, *Opt. Lett.* **38**, 1912 (2013).
- [63] S. Weimann, M. Kremer, Y. Plotnik, Y. Lumer, S. Nolte, K. G. Makris, M. Segev, M. C. Rechtsman, and A. Szameit, *Nature materials* **16** **4**, 433 (2017).
- [64] Other choices could also be considered, but with less experimental relevance and a more complicated interpretation in terms of mutual information [49].
- [65] I. Peschel, *Journal of Physics A: Mathematical and General* **36**, L205 (2003).
- [66] D. Wang, S. Xu, Y. Wang, and C. Wu, *Phys. Rev. B* **91**, 115118 (2015).
- [67] G. B. Mbeng, A. Russomanno, and G. E. Santoro, *SciPost Phys. Lect. Notes* , 82 (2024).
- [68] The standard definition by Kitaev, which in row-vector form would read:

$$\begin{aligned} \check{c} &= (\check{c}_1, \check{c}_2, \check{c}_3, \check{c}_4, \dots, \check{c}_{2N-1}, \check{c}_{2L})^T \equiv \\ &\equiv (\check{c}_{1,1}, \check{c}_{2,1}, \check{c}_{1,2}, \check{c}_{2,2}, \dots, \check{c}_{1,N}, \check{c}_{2,L})^T, \end{aligned} \quad (\text{F10})$$

mixes the different blocks of the Nambu fermions in a way that makes the algebra more complicated.

- [69] T. Prosen, *Journal of Statistical Mechanics: Theory and Experiment* **2010**, P07020 (2010).
- [70] T. Prosen, *New Journal of Physics* **10**, 043026 (2008).
- [71] A. Kitaev, *AIP Conference Proceedings* **1134**, 22 (2009).
- [72] C.-K. Chiu, J. C. Y. Teo, A. P. Schnyder, and S. Ryu, *Rev. Mod. Phys.* **88**, 035005 (2016).
- [73] J. Surace and L. Tagliacozzo, *SciPost Phys. Lect. Notes* , 54 (2022).
- [74] L. M. Sieberer, M. Buchhold, J. Marino, and S. Diehl, (2023), [arXiv:2312.03073](https://arxiv.org/abs/2312.03073).
- [75] G. Passarelli, V. Cataudella, and P. Lucignano, *Phys. Rev. B* **100**, 024302 (2019).
- [76] N. Friis, *New Journal of Physics* **18**, 033014 (2016).
- [77] N. Friis, A. R. Lee, and D. E. Bruschi, *Phys. Rev. A* **87**, 022338 (2013).